2126–2143 *Nucleic Acids Research, 2020, Vol. 48, No. 4* *Published online 21 December 2019*
doi: 10.1093/nar/gkz1168

The conserved 3′ UTR-derived small RNA NarS mediates mRNA crossregulation during nitrate respiration

Chuan Wang [1,2,*], Yanjie Chao [2,3], Gianluca Matera[2], Qian Gao[1] and Jörg Vogel[2,4,*]

[1]Key Laboratory of Medical Molecular Virology (MOE/NHC/CAMS), School of Basic Medical Sciences, Shanghai Medical College, Fudan University, Shanghai 200033, PR China, [2]Institute for Molecular Infection Biology, University of Würzburg, D-97080 Würzburg, Germany, [3]Howard Hughes Medical Institute, Department of Molecular Biology and Microbiology, Tufts University School of Medicine, Boston, MA 02111, USA and [4]Helmholtz Institute for RNA-based Infection Research (HIRI), Helmholtz Center for Infection Research (HZI), D-97080 Würzburg, Germany

Received August 15, 2019; Revised November 27, 2019; Editorial Decision November 29, 2019; Accepted December 02, 2019

ABSTRACT

Small noncoding RNAs (sRNAs) from mRNA 3′ UTRs seem to present a previously unrecognized layer of bacterial post-transcriptional control whereby mRNAs influence each other's expression, independently of transcriptional control. Studies in *Escherichia coli* and *Salmonella enterica* showed that such sRNAs are natural products of RNase E-mediated mRNA decay and associate with major RNA-binding proteins (RBPs) such as Hfq and ProQ. If so, there must be additional sRNAs from mRNAs that accumulate only under specific physiological conditions. We test this prediction by characterizing candidate NarS that represents the 3′ UTR of nitrate transporter NarK whose gene is silent during standard aerobic growth. We find that NarS acts by Hfq-dependent base pairing to repress the synthesis of the nitrite transporter, NirC, resulting in mRNA cross-regulation of nitrate and nitrite transporter genes. Interestingly, the NarS-mediated repression selectively targets the *nirC* cistron of the long *nirBDC-cysG* operon, an observation that we rationalize as a mechanism to protect the bacterial cytoplasm from excessive nitrite toxicity during anaerobic respiration with abundant nitrate. Our successful functional assignment of a 3′ UTR sRNA from a non-standard growth condition supports the notion that mRNA crossregulation is more pervasive than currently appreciated.

INTRODUCTION

Genes are generally controlled in a vertical manner such that input signals cause changes in their transcription or in the synthesis of regulatory factors that then affect their expression on the post-transcriptional or post-translational levels. Over the past decade, however, evidence has accumulated in both eukaryotes and prokaryotes for mechanisms of additional gene regulation whereby an mRNA directly influences another without changes in transcription (1). In bacteria, mRNA crosstalk most prominently starts by mRNA decay releasing the 3′ untranslated region (3′ UTR) of one mRNA as a small regulatory RNA (sRNA) that is then free to interact with the 5′ end of another mRNA (2–9). The base pairing typically sequesters the ribosome binding site (RBS) of the target mRNA, inhibiting translation, and in the model bacteria *Escherichia coli* and *Salmonella enterica* typically requires one of two major RBPs, Hfq or ProQ (10–13).

Originally observed as a curiosity in early genome-wide sRNA screens (14–16), stable RNA fragments from the 3′ end of protein-coding genes have recently emerged as a potentially large group of overlooked post-transcriptional regulators. Specifically, RNA-seq showed such mRNA 3′ fragments to be very abundant amongst Hfq-associated cellular RNA species (17). Since the cellular concentration of Hfq is limiting, its RNA ligands are assumed to be enriched for functional regulatory RNAs (18,19).

There are two general types of 3′ end-derived sRNAs: the first are sRNAs such as DapZ (17) and MicL (20) that are transcribed from an independent sRNA gene hidden within the 3′ end of a protein-coding gene on the same strand. They use an ORF-internal promoter but share the transcription terminator with the mRNA. Here, we focus on the other type: 3′ UTR-derived sRNAs that are generated by 3′ end cleavage of mRNAs and often comprise just the 3′ UTR

*To whom correspondence should be addressed. Tel: +49 931 3182575; Email: joerg.vogel@uni-wuerzburg.de
Correspondence may also be addressed to Chuan Wang. Email: chuanwang@fudan.edu.cn

of the latter. They have been described in several different bacteria and physiological pathways (2,21,22), with the majority of studies coming from *E. coli* and *Salmonella*.

A primary example of a 3′ UTR-derived sRNA is CpxQ (3,4). Clipped off the mRNA of membrane stress chaperone CpxP, CpxQ acts to translationally repress multiple mRNAs of extracytoplasmic proteins in the inner membrane stress response. The post-transcriptional repressor activity of the CpxQ sRNA is to limit *de novo* synthesis of these potentially problematic proteins while the CpxP protein that is synthesized from the same mRNA acts on the misfolded proteins that have already accumulated (3,4). Further examples are SroC and SdhX from the *gltI* and *sucD* mRNAs, respectively (7,8,14,23). Similarly to CpxQ, both of these sRNAs regulate other transcripts by conserved, Hfq-dependent base pairing: SroC acts as a sponge of the major sRNAs GcvB and MgrR (23,24), while SdhX links the TCA cycle with acetate metabolism by repressing the synthesis of acetate kinase AckA (7,8). By contrast, RaiZ is an example of an Hfq-independent sRNA; it originates from the 3′ UTR of *raiA* (ribosome inactivating protein) mRNA and associates with the alternative global RBP ProQ to translationally inhibit the mRNA of histone-like protein HU (6). In all of the above examples, the nuclease responsible for sRNA biogenesis is RNase E, the major endoribonuclease of Gram-negative bacteria (25–27). Together, these findings have established endonucleolytic mRNA cleavage as an alternative pathway that produces Hfq- and ProQ-dependent sRNAs in addition to classic sRNA biogenesis from noncoding genes.

A major open question regarding 3′ UTR-derived sRNAs is their actual number. RNase E cleavage sites are enriched around mRNA stop codons (28), therefore mRNA turnover by this nuclease *per se* releases thousands of 3′ UTR fragments in *E. coli* and *Salmonella*. Many of these 3′ fragments contain a Rho-independent transcription terminator, i.e., a structure that attracts the sRNA chaperones Hfq or ProQ (29–31). In addition, the examples of SdhX and RaiZ demonstrate that even 3′ UTRs with very little conserved primary sequence give rise to functional sRNAs; in both sRNAs, only the short seed sequence is well-conserved (6,7). Together, these observations indicate that more 3′ UTRs than currently appreciated may produce functional sRNAs. For example, of the 61 candidates predicted from a combination analysis of global RNase E site mapping by TIER-seq (transiently inactivating an endoribonuclease followed by RNA-seq) and Hfq co-immunoprecipitation (coIP) (17,28), only 14 were properly annotated as sRNAs in the *Salmonella* transcriptome (32). The other candidates usually show very low expression under the standard culture condition, i.e., aerobic culture in LB broth (33).

To address whether the large pool of processed 3′ UTRs with low cellular copy numbers contains more *bona fide* riboregulators, we chose to analyze the seemingly low-confidence candidate NarS. Previously known as *Salmonella* STnc2040 (33), NarS represents the 3′ UTR of the mRNA of nitrate (NO_3^-) transporter NarK and shows low expression, low conservation of primary sequence. It is also shorter than most sRNAs with an established function. Here, we have identified the mRNA of nitrite (NO_2^-) transporter NirC as a conserved cellular target of NarS, suggesting that this sRNA plays a role in the homeostasis of cytoplasmic nitrate respiration under oxygen-limiting growth conditions. Interestingly, the NarS-mediated repression of *nirC* spares the genes of a nitrite reductase (*nirBD*) that are encoded by the same operon mRNA. In other words, NarS helps to deal with the conflicting expression of a nitrate transporter and nitrite transporter while the synthesis of nitrite reductase must also be ensured. By assigning a physiological role to NarS, our study supports the notion that more bacterial 3′ UTR sRNAs displaying limited sequence conservation and low copy number regulate gene expression on the mRNA level.

MATERIALS AND METHODS

Bacterial strains and growth conditions

A complete list of bacterial strains used in this study is provided in Supplementary Table S1. *Salmonella enterica* serovar Typhimurium strain SL1344 (QGS-001) is referred to as wild type and was used for mutant construction. Bacteria were grown at 37°C with continuous shaking at 220 rpm in Luria-Bertani (Oxoid™) or M9CA minimal medium supplemented with 0.4% glucose and 20 mM sodium nitrate.

Overnight cultures were grown from a single colony, diluted 1:100 in fresh medium, and grown to the indicated OD_{600}. Where appropriate, media were supplemented with antibiotics at the following concentrations: 100 μg/ml ampicillin (Amp), 50 μg/ml kanamycin (Kan) and 20 μg/ml chloramphenicol (Cm). Unless stated otherwise, chemicals were purchased from Sangon Biotech, Shanghai. For anaerobic shock (33), cells were aerobically cultured to an OD_{600} of 0.3, filled in 50 ml closed Falcon tubes, and incubated without agitation at 37°C for the indicated time. For heat shock in the *rne*-TS experiment, bacteria were grown in LB at 28°C to an OD_{600} of 0.3, and then grown for 30 min at 28°C or 44°C in sealed Falcon tubes (anaerobic shock condition).

Strain construction

Deletion strains and chromosomally 3xFLAG epitope-tagged strains were constructed using the λ-Red recombinase one-step inactivation method (34,35). As exemplified by QGS-325 (Δ*narK*ΔNarS) and QGS-479 (*nirC::3xflag*), *Salmonella* wild-type cells carrying the pKD46 helper plasmid were transformed with 1 μg DNA fragments to be integrated, which were amplified from pKD4 using QGO-634/-636 (Δ*narK*ΔNarS), or from pSUB11 using QGO-651/-652 (*nirC::3xflag*). The correct insertions of the Kan^R marker gene were verified by PCR using QGO-637/-638 or QGO-653/-654, respectively. Phage P22 was used to transduce chromosomal modifications to fresh wild-type background. To eliminate the resistance genes from chromosome, strains were transformed with the temperature-sensitive plasmid pCP20 expressing FLP recombinase. Mutants that were susceptible to kanamycin and ampicillin were selected on LB agar plates at 37°C by duplicate plating. Finally,

chromosomal modifications were confirmed by PCR using QGO-637/-638 or QGO-653/-654, and by Sanger sequencing of the PCR products.

DNA/RNA oligonucleotides and plasmids

All the plasmids used in this study including a brief description of their construction are summarized in Supplementary Table S2. Sequences of all the oligonucleotides employed in this study are listed in Supplementary Table S3. Competent *E. coli* DH5α (#CB101, TIANGEN Biotech) were used for cloning. Plasmids were isolated using TIANprep Rapid Mini Plasmid Kit (#DP105, TIANGEN Biotech) and confirmed by Sanger sequencing.

Sequence alignments

Nucleotide alignments of homologous sequences were performed using Nucleotide Blast searches (https://blast.ncbi.nlm.nih.gov/Blast.cgi) using the following genomes: *Salmonella* Typhimurium LT2 (NC_003197), *Salmonella* Typhi Ty2 (NC_004631), *Citrobacter koseri* ATCC BAA-895 (NC_009792), *E. coli* K12 *MG1655* (NC_000913), *Shigella flexneri* 2a str 301 (NC_004337), *Enterobacter* sp. 638 (NC_009436), *Cronobacter turicensis* z30232 (NC_013282), *Leclercia* sp. LSNIH1 (NZ_CP026167.1), *Cedecea lapagei* NCTC11466 (LR134201.1). Alignments were generated with MultAlin at http://multalin.toulouse.inra.fr/multalin/multalin.html.

RNA isolation and Northern blot analysis

Bacterial cultures were mixed with 0.2 volumes of stop solution (95% ethanol and 5% phenol) and immediately frozen in liquid nitrogen. Total RNA was isolated using the hot phenol method. Briefly, 2.0 OD_{600} of cells were resuspended with 300 μl lysozyme (#L3790, Sigma-Aldrich) at 0.5 mg/ml, 30 μl 10% SDS and 33 μl 3M sodium acetate (pH5.2). Cleared lysate was mixed with 375 μl saturated phenol (pH4.5) and incubated at 64°C for 6 min with shaking. After mixing with 375 μl chloroform and centrifugation in a Phase Lock Gel tube (#WM5-2302820, TIANGEN Biotech), the aqueous phase was collected for RNA precipitation. RNA was precipitated at −80°C overnight by mixing the aqueous phase (∼350 μl) with 700 μl 30:1 ethanol:sodium acetate (pH 6.5) mix. RNA pellets were washed with 80% ethanol and dissolved in ultra-pure water (#10977, Thermo Fisher Scientific). RNA concentration was determined using NanoDrop 2000.

For polyacrylamide gels, 10 μg of total RNA was denatured at 95°C for 2 min in RNA gel loading buffer II (95% formamide, 18 mM EDTA, 0.025% SDS, 0.025% xylene cyanol, 0.025% bromophenol blue), and separated by gel electrophoresis on 6% polyacrylamide/7 M urea gels in 1× TBE buffer for 2 h at 300 V using Beijing Liuyi DYCZ system (Beijing Liuyi Biotechnology). RNA was transferred from gels onto Hybond-N+ membranes (GE Healthcare) by electroblotting for 2 h at 25 V at 4°C. For agarose gels, 25 μg of total RNA was denatured at 65°C for 5 min in RNA loading buffer (30.84% deionized formamide, 2.7% formaldehyde, 2 mg/ml bromophenol blue, 4× MOPS, 4 mM EDTA pH 8.0 and 20% glycerin), and separated in 1.2% agarose gel containing 1% formaldehyde in 1x MOPS buffer for 1.5 h at 125 V using the Tanon HE120 system (Tanon Science & Technology). Gels were stained with ethidium bromide to visualize rRNA, then transferred onto Hybond-N+ membranes (#RPN203S, GE Healthcare) using capillary blotting in 10x SSC buffer overnight. The membranes were cross-linked with UV light (120 mJ/cm^2).

Northern blot analysis was performed using the Roche DIG system. Briefly, membranes were prehybridized in DIG Easy Hyb (#11796895001, Roche) for 30 min. Digoxin-labeled DNA probe (OGO-702 for probing NarS) was hybridized at 50°C overnight. Digoxin-labelled RNA probe was hybridized at 68°C overnight. Membranes were washed in three 15-min steps in 5× SSC/0.1% SDS, 1× SSC/0.1% SDS and 0.5× SSC/0.1% SDS buffers at 50°C for DNA probe or 68°C for RNA probe. Following one wash in maleic acid wash buffer (0.1 M maleic acid, 0.15 M NaCl, 0.3% Tween-20 pH 7.5) for 5 min at 37°C and blocked with blocking solution (#11585762001, Roche) for 45 min at 37°C, membrane was hybridized with 75 mU/ml Anti-Digoxigenin-AP (#11093274001, Roche) in blocking solution for 45 min at 37°C. Membranes were then washed again in maleic acid wash buffer in two 15-min steps and equilibrated with detection buffer (0.1 M Tris–HCl, 0.1 M NaCl, pH 9.5). Signals were visualized by CDP-star (#12041677001, Roche) on a ChemiDocTM XRS+ station and quantified using ImageLabTM Software (both Biorad).

GFP fluorescence quantification

Salmonella strains carrying (superfolder) GFP translational fusions (36) were grown in LB containing Amp and Cm to an OD_{600} of 0.5. 100 μl cultures were collected and washed three times with 1× PBS before fixing with 4% paraformaldehyde. GFP fluorescence intensity was quantified by flow cytometry (FACS Calibur, BD Bioscience).

Western blot analysis

Western blot was performed as described (3,37). Briefly, 0.1 OD_{600} bacterial culture was collected by centrifugation for 2 min at 8000 rpm at 4°C, and resuspended in 100 μl 1× protein loading buffer. After heating for 5 min at 95°C, 0.02 OD_{600} of cell lysate was separated on a 10% SDS-PAGE gel. Proteins were transferred onto a NC membrane (#10600002, GE Healthcare) for 60 min at 100 V in transfer buffer (25 mM Tris, 190 mM glycine, 20% methanol, pH 8.3). Membranes were blocked for 1 h at room temperature in 1× TBST (20 mM Tris, 150 mM NaCl, 0.1% Tween20, pH 7.6) buffer with 5% (w/v) Difco™ skim milk (#6307915, BD). After blocking, membranes were incubated at room temperature for 1 h with monoclonal α-FLAG (Sigma-Aldrich #F1804; 1:1000) or polyclonal α-GroEL (Sigma-Aldrich #G6532; 1:5000) antibodies diluted in 1× TBST buffer containing 3% BSA. Following three washes for 30 min in 1× TBST buffer, membranes were incubated with secondary α-mouse or α-rabbit HRP-linked antibodies (Sigma-Aldrich #A0168 or #A0545; 1:5000)

diluted in 1× TBST buffer containing 3% BSA. After another three washes for 30 min in 1× TBST buffer, chemiluminescence was developed using the Novex™ ECL Chemiluminescent Substrate Reagent Kit (#WP20005, Thermo Fisher Scientific), visualized on ChemiDocTM XRS+, and quantified using ImageLabTM Software (both Biorad).

Quantitative PCR

Quantitative PCR was performed with the PrimeScript™ RT reagent Kit (#RR047A, Takara Bio). Briefly, 1 μg total RNA was treated with gDNA eraser provided in the kit at 42°C for 2 min, and then reverse-transcribed to cDNA with random oligos and PrimeScript RT Enzyme Mix I at 37°C for 15 min. cDNA transcribed from 0.025 μg total RNA was used per PCR reaction in a final volume of 20 μl with TB Green Premix Ex Taq II (#RR820A, Takara Bio). PCR was performed using a Biorad CFX96 Touch Real-Time PCR Detection System. Data were analyzed with relative quantification (ddCt) method. The *rfaH* gene was used as reference gene for normalization.

RNA sequencing

RNA-seq was performed by BGI Group, Shenzhen, Guangdong, China. Briefly, a strand-specific cDNA library was constructed for each sample to keep the direction of RNA transcription. The obtained cDNA libraries were sequenced on Illumina HiSeq 4000. Adaptors were removed and quality of RNA-seq data was assessed by SOAP software package (38). High-quality reads were mapped to the genome of *Salmonella* strain SL1344 using HISAT software package (39). Relative expression of each individual gene was calculated in each sample by counting fragments per kilobase of transcript per million mapped reads (FPKM) with Bowtie2 and RSEM software packages (40,41). Sequencing data have been deposited with NCBI Gene Expression Omnibus (GEO) under accession number GSE135757.

In vitro RNA synthesis and RNA labelling

For *in vitro* synthesis of NarS and *nirC* 5′ UTR transcripts, 200 ng of a DNA fragment amplified from *Salmonella* genomic DNA (using primer pair QGO-782/784 for NarS, QGO-843/844 for *nirC* 5′ UTR) served as template in a T7 transcription reaction using the MEGAscript™ T7 Transcription Kit (#AM1334, Thermo Fisher Scientific). The correct size and integrity of RNA were confirmed in a denaturing polyacrylamide gel. RNA bands were excised from gel and eluted with 0.1 M sodium acetate, 0.1% SDS, 10 mM EDTA at 4°C overnight, followed by Phenol:Chloroform:Isoamyl isolation and precipitation. To create digoxin-labeled RNA probe for northern blotting, 200 ng of a DNA fragment amplified from *Salmonella* gDNA (using primer pair QGO-818/819 for anti-*cysG* probe, QGO-822/823 for anti-*nirB* probe, QGO-841/842 for anti-*narK* probe) served as template in a T7 transcription reaction using the DIG RNA Labeling Kit (#11175025910, Roche). For radio-labelling, 50 pmol RNA was dephosphorylated with 10 units of calf intestine alkaline phosphatase (#M0290, New England Biolabs) in a 50 μl reaction at 37°C for 1 h, followed by phenol:chloroform:isoamyl isolation and precipitation. 20 pmol dephosphorylated RNA was 5′-labeled with 3 μl of ^{32}P-γ-ATP (10 Ci/l, 3000 Ci/mmol) using 1 unit of T4 polynucleotide kinase (#EK0031, Thermo Fisher Scientific) for 1 h at 37°C in a 20 μl reaction. Microspin G-50 columns (#27533001, GE Healthcare) were used to remove unincorporated nucleotides according to the manufacturer's instructions.

Protein purification and electrophoretic mobility shifts assays

Salmonella Hfq purification was performed by intein-based expression (IMPACT, New England Biolab) as described before (42). For EMSA, 5 nM of radio-labeled RNA was used in each reaction. Labeled RNA was denatured at 95°C for 2 min, chilled on ice for 5 min and mixed with purified Hfq protein at different concentrations in a final volume of 10 μl of 10 mM Tris–HCl, pH 7, 100 mM KCl, 10 mM $MgCl_2$. Reactions were incubated at 37°C for 10 min, stopped by adding 5× RNA native loading buffer, and resolved on native 8% polyacrylamide gels at 4°C in 0.5× TBE at constant current of 40 mA for 4 h. Gels were dried and signals were analyzed on a Typhoon FLA 7000 phosphoimager using AIDA software.

RNA structure probing and Hfq footprinting assays

Structure probing and Hfq footprinting were performed with *in-vitro* transcribed 5′-radio-labeled RNA as described (6). Briefly, 0.2 pmol labeled RNA (in 5 μl) was denatured at 95°C for 2 min and chilled on ice for 5 min, followed by the addition of 1 μl of yeast RNA (1 mg/ml, #AM7118, Thermo Fisher Scientific) and 1 μl of 10× structure buffer (0.1 M Tris–HCl, pH 7, 1 M KCl, 0.1 M $MgCl_2$). Unlabeled partner RNA or Hfq protein were then added and incubated at 37°C for 10 min. Samples were treated with 0.1 U RNase T1 (#AM2283, Thermo Fisher Scientific) for 3 min, or with 5 mM lead (II) acetate (Fluka) for 1.5 min, respectively. RNase T1 sequencing ladders were prepared by using 0.4 pmol 5′-labeled RNA digested with 0.1 U RNase T1 for 5 min at 37°C. Alkaline (OH) sequencing ladders were prepared by incubating 0.4 pmol 5′-labeled RNA at 95°C for 5 min in the presence of alkaline hydrolysis buffer. Reactions were stopped by adding 12 μl RNA Gel loading buffer II. Samples were denatured at 95°C for 2 min and separated on denaturing 8% sequencing gels containing 7 M urea in 1× TBE at constant power of 40 W for 1 h. Gels were dried and signals were analyzed on a Typhoon FLA 7000 phosphoimager using AIDA software.

5′ RACE

5′-RACE experiments followed described protocols (36) with a few modifications. Briefly, 5 μg of total DNA-free RNA was treated with 20 U of RNA 5′ polyphosphatase (RP8092H, Epicentre) in a total volume of 20 μl at 37°C for 30 min. Following Phenol:Chloroform:Isoamyl extraction, RNA was precipitated from the aqueous phase together

with 250 pmol of RNA adapter A4 using three volumes of 30:1 ethanol:sodium acetate (pH 6.5) mix. For ligation of the RNA linker, the RNA pellet was resuspended in ultra-pure water and allowed to dissolve for 10 min at 65°C, after which a 20 μl reaction containing 20 U T4 RNA ligase (#EL0021, Thermo Fisher Scientific), 1× T4 RNA ligase buffer, 10% (v/v) DMSO and 10 U SUPERaseIn RNase Inhibitor (#AM2694, Thermo Fisher Scientific) was incubated at 16°C overnight. Following Phenol:Chloroform:Isoamyl extraction and ethanol precipitation, the ligated RNA was reverse-transcribed using random hexamer primers (#N8080127, Thermo Fisher Scientific) and 200 U Superscript III reverse transcriptase (#18080085, Thermo Fisher Scientific) in a 20 μl reaction mix containing 1× FS buffer, 2 mM dNTPs, 5 mM DTT and 10 U SUPERaseIn RNase Inhibitor. Template RNA was digested with RNase H (#EN0201, Thermo Fisher Scientific). To identify the 5′ end of genes, 1 μl aliquots of the RT reaction were used as templates in a PCR reaction with 1 mM linker-specific primer RACE-Fw and gene-specific primers including QGO-757 (*cysG*), QGO-832 (*nirB*), QGO-833 (*nirD*) and QGO-835 (*nirC*). PCR was performed with Taq DNA polymerase (#KT211, TIANGEN Biotech). The PCR products were resolved in 3% agarose gels. Selected bands were purified and cloned in T-Vector pMD™19 (#3271, Takara Bio). Inserts of obtained clones were analyzed by Sanger sequencing.

Extracellular nitrite concentrations assay

Bacterial cells were grown in M9CA medium supplemented with 0.4% glucose to an OD_{600} of 0.3, and then supplemented with sodium nitrate (final concentration: 20 mM). Cultures were transferred to 15 ml closed Falcon tubes and incubated without agitation. At indicated time points, tubes were centrifuged without opening. 50 μl supernatant each tube was removed and immediately analyzed to determine the nitrite concentration using a colorimetric assay as described (43). Briefly, 50 μl supernatant was mixed with 50 μl of 1% (w/v) sulphanilamide (#251917, Sigma-Aldrich) in 1 M HCl and 50 μl of 0.02% (w/v) naphthylethylene diamine dihydrochloride (#33461, Sigma-Aldrich). Absorbance at 540 nM was read on a Biorad benchmark plus microplate reader. Serial dilutions of defined sodium nitrite in M9CA medium were used to draw a standard curve for calculating the nitrite concentration in tested cultures.

RESULTS

Expression levels of 3′ UTR-derived versus canonical sRNAs

To obtain a better picture of the cellular levels of 3′ UTR-derived sRNAs, we analyzed known and candidate *Salmonella* sRNAs from Hfq CoIP and CLIP-seq data (17,44) with respect to their absolute expression levels during aerobic growth in LB-broth. To this end, expression data from mid-exponential and early stationary phase were collected from the Salcom website (33) and calculated as transcripts per million (Figure 1 and Supplementary Table S4). We double-checked RNase E processed 3′ UTR candidates (red bars in Figure 1) against two data sets: differential RNA-seq data (32) to test for the presence of a potential transcription start site (TSS) near the 3′ end of a coding gene; and TIER-seq data (28) to check for an RNase E cleavage site at the 5′ end of an sRNA. Those located near the 3′ end of a coding gene without annotated TSS but with an RNase E cleavage sites are defined as processed 3′ UTR sRNA candidates.

We did not find a single RNase E processed 3′ UTR sRNA at the high end of the expression range. In fact, the top 10 sRNAs accounting for nearly 85% of total transcripts of Hfq-bound sRNAs are all well-characterized sRNAs (except STnc710) with independent promoters, at least under the two growth conditions investigated. The RNase E processed 3′ UTR candidates only account for <7% (∼4.45% in mid-exponential phase, ∼6.57% in early stationary phase) of all reads. Of these, almost a quarter come from CpxQ (a.k.a. STnc870). Calibration of the RNA-seq data with experimentally determined sRNA copy numbers for the *Salmonella* DapZ, InvR and SdsR sRNAs (17,45,46) leads us to predict that the copy numbers of many RNase E processed 3′ UTR sRNAs may well be <1 per cell (equal to ∼300 transcripts per million reads) in these two growth phases. This would include sRNAs such as NarS (STnc2040), STnc2010, STnc2110 and STnc2160 that otherwise show high enrichment in Hfq coIP. However, we also noticed that the expression of those low-abundance sRNAs was considerably higher in more specialized growth conditions. In particular, Salcom predicted that NarS levels increased by ∼71 fold upon change to anaerobic growth (Supplementary Figure S1). Thus, NarS seemed a promising candidate for a low-abundance, RNase E processed 3′ UTR candidates that may reveal its function only under non-standard conditions.

NarS is a new Hfq-dependent sRNA derived from the 3′ UTR of *narK* mRNA

The sRNA in question was originally identified as candidate STnc2040 by RNA-seq of Hfq ligands in *Salmonella* (17); we renamed it here NarS for 'nitrate respiration-related sRNA' to reflect its origin in the 3′ UTR of *narK*, a gene that encodes a nitrate/nitrite transporter involved in nitrate respiration. According to *Salmonella* dRNA-seq data, its major form is a 63 nt RNA which we will refer to as NarS-S; the *E. coli* K12 counterpart is longer (∼230 nt) due to a 170-nt insertion sequence near the *narK* stop codon (33,47). NarS sequences are found in the *narK* locus of a sub-clade of the *Enterobacteriaceae* that comprises *Citrobacter*, *Salmonella*, *Escherichia*, *Shigella*, *Enterobacter*, *Leclercia, Cronobacter* and *Cedecea* (Figure 2A, Supplementary Figure S2). Under the assumption of maximum parsimony, NarS seemed to have been gained as this sub-clade separated from the ancestral core of *Erwinia*/*Pantoea*. A NarS sequence alignment revealed a short stretch of highly conserved, likely single-stranded bases upstream of the terminator hairpin, a configuration reminiscent of the seed sequence for target pairing in well-characterized Hfq-dependent sRNAs (48,49).

We confirmed by northern blotting and RT-qPCR, respectively, the prediction by Salcom (33) that NarS and *narK* are upregulated during anaerobic respiration. We

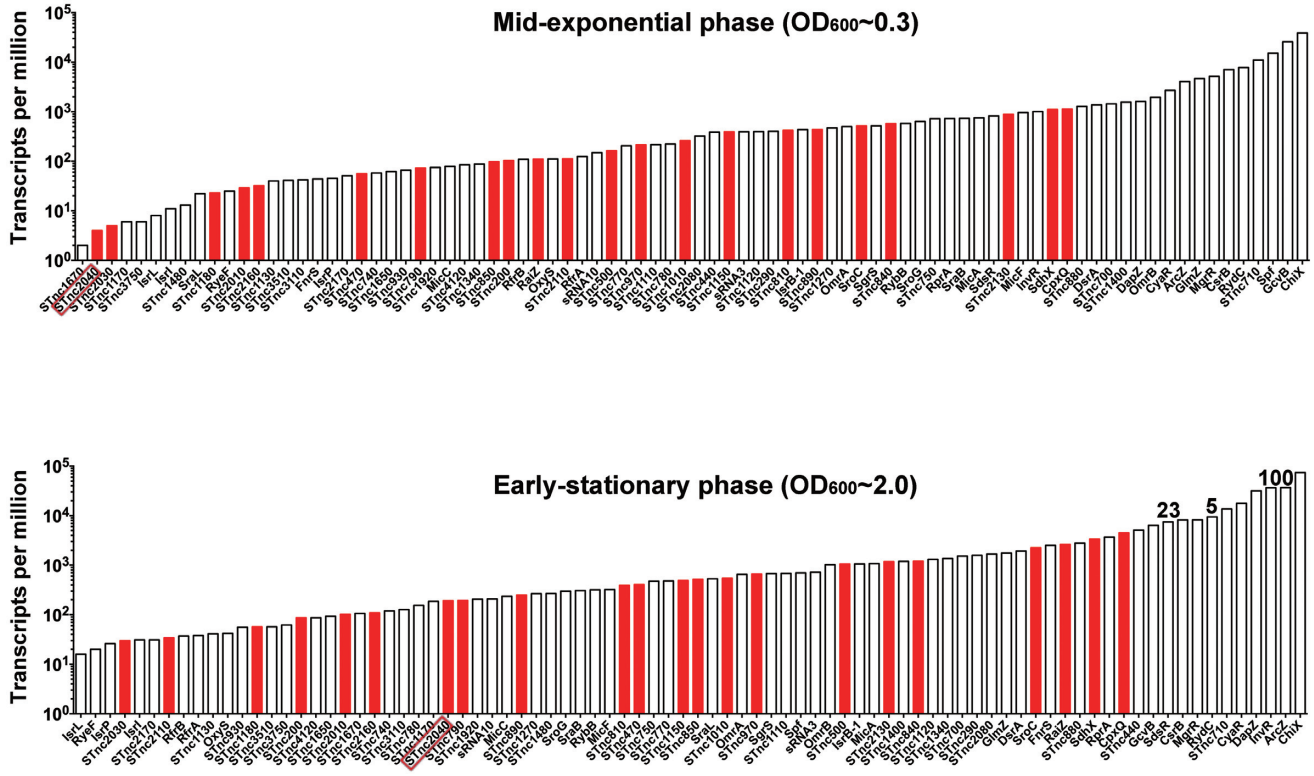

Figure 1. Cellular abundance of different types of *Salmonella* Hfq-dependent sRNAs. Expression of Hfq-bound sRNAs in mid-exponential (top) or early stationary phase (bottom) in LB-broth. The list of Hfq-bound sRNAs was generated from Hfq-CoIP and Hfq-CLIP data (17,44). Expression values calculated as transcripts per million collected from the Salcom database (Supplementary Table S4) (33). The RNase E processed 3′ UTR candidates were predicted with TIER-seq data (28) and are marked in red. Experimentally confirmed copy numbers of sRNAs (17,45,46) are given above.

observed a very strong (3,349 ± 129-fold) induction of *narK* following 10 min of anaerobic shock (Supplementary Figure S3A). NarS was also strongly induced by anaerobic shock (Figure 2B), with a short delay after the *narK* mRNA but with sustained high levels over the course of two hours. In addition to the main NarS-S species, the oligonucleotide probe used here detected a ∼110 nt RNA species to which we will refer as NarS-L. Its weak signal suggests that it is a precursor of NarS-S, representing a longer processing intermediate of the *narK* mRNA. However, NarS-S clearly constitutes the major NarS form, hence we focused our functional characterization on it.

There was prior evidence that NarS is an Hfq-associated sRNA: strong enrichment in Hfq coIP in both *E. coli* and *Salmonella* (17,47) and Hfq-dependent crosslinking (positions marked in Figure 2C) in UV CLIP-seq (44). By contrast, NarS does not seem to associate with the other two major sRNA-related RBPs, CsrA and ProQ (31,44). Further supporting Hfq dependence, NarS is almost undetectable in a *Salmonella* Δ*hfq* strain (Figure 3A) and its half-life without Hfq drops to <1 min from >8 min when expressed from a plasmid (Supplementary Figure S4A). In an Electrophoretic Mobility Shift Assay (EMSA), Hfq formed a stable complex with *in vitro*-synthesized NarS (Supplementary Figure S4B); the observed apparent K_d of ∼10 nM is similar to other well-characterized Hfq-associated sRNAs (18,50,51). *In-vitro* RNA footprinting indicated that Hfq protects the poly-U tail at the 3′ end of NarS (Supplementary Figure S4C) where it may inhibit sRNA degradation by 3′→5′ exoribonucleases (52). Taken together, NarS exhibits diverse molecular features of Hfq-associated sRNAs, suggesting that this processed 3′ UTR of *narK* may act in the cell to regulate other transcripts.

Previous work in *E. coli* suggested that most nitrate respiration genes are transcriptionally controlled by the global regulator FNR as well as the two-component systems, NarX/L and NarQ/P (53–56). Taking this as a starting point to understand how *narK* and NarS were regulated, we constructed *Salmonella* strains lacking each of these factors and observed drastically reduced expression of *narK* and almost total loss of NarS in single mutants lacking NarL or FNR (Figure 3A, Supplementary Figure S3B). By contrast, loss of NarP had almost no effect on the *narK* mRNA or NarS. In conclusion, NarS and its parental gene *narK* are transcriptionally activated by NarX/L and FNR, similar to many other genes in the nitrate respiration pathway.

RNase E liberates NarS from the *narK* mRNA

Regarding NarS biogenesis, the available *Salmonella* RNA-seq data offered conflicting predictions: TIER-seq predicted that NarS was an RNase E cleavage product with a monophosphorylated 5′ end (28), whereas dRNA-seq datasets predicted NarS was a primary transcript with a triphosphorylated 5′ end (32). Here, several independent

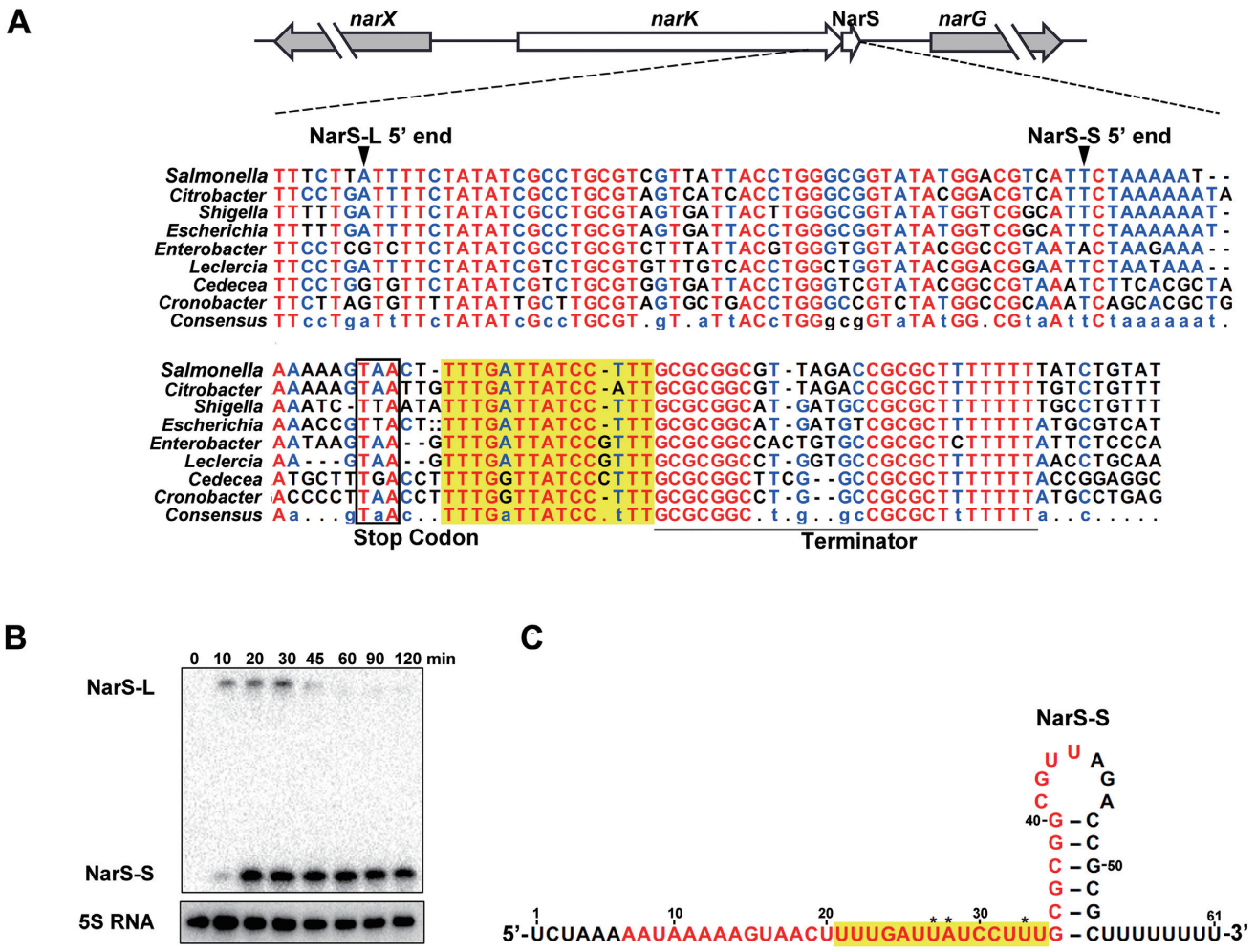

Figure 2. NarS is a 3′ UTR derived sRNA from nitrate transporter gene *narK*. (**A**) Genomic context of *narK* and NarS. Alignment of *narK* 3′UTRs of selected enterobacterial genera is shown below. Conserved nucleotides are marked in red. The stop codon of the *narK* ORF is boxed. The Rho-independent terminator is underlined and potential seed-sequence is highlighted. '::' near the stop codon in the *E. coli* sequences (*Escherichia*) represents a 170-nt insertion. (**B**) Expression of NarS in *Salmonella* under anaerobic shock. *Salmonella* SL1344 cells were grown to OD_{600} of 0.3 in LB broth, then filled into 50 ml closed Falcon tube and incubated without agitation at 37°C for 2 h. Total RNA was isolated at indicated time points post treatment and analyzed on a northern blot. 5S RNA was probed as a loading control. (**C**) Predicted secondary structure of NarS-S. Hfq-binding regions identified by UV CLIP-seq analysis are marked with red letters. UV-crosslinking induced mutations are indicated by asterisks. The potential seed sequence is highlighted in yellow.

experiments confirmed the former prediction, i.e. both NarS-S and the NarS-L precursor are processed RNA species. First, deleting either the entire *narK* 5′ region (Δ*narK*ΔNarS) or just the *narK* promoter (ΔP_{narK}) abrogated NarS expression (Figure 3B, lanes 2 and 3), suggesting that NarS expression is dictated by the *narK* promoter. Second, a deletion of the *narK* promoter and ORF while retaining NarS including 100 bps upstream sequence ($\Delta P_{narK}\Delta narK$) also abrogated NarS expression (Figure 3B, lane 4); reciprocally, cloning NarS including 100 bps upstream region in a high-copy plasmid yielded no sRNA expression (Figure 3C), all of which argues against the presence of an internal promoter in the 3′ region of *narK*. Third, truncating the *narK* ORF did not interfere with NarS expression (Figure 3B, line 5, Δ*narK*), suggesting that NarS production is solely determined by sequences in the 3′ end of the *narK* mRNA. Collectively, these results robustly establish that NarS results from 3′ processing of the primary *narK* transcript.

To determine the role of RNase E in NarS biogenesis, we probed for NarS in an RNase E thermo-sensitive mutant of *Salmonella* (*rne*-TS or *rne-3071*; (57,58)). Figure 3D shows that upon inactivation of RNase E by shift to non-permissive 44°C, NarS disappeared whereas full-length *narK* mRNA accumulated (Supplementary Figure S5). Thus, RNase E processes the primary *narK* mRNA into the NarS-L precursor as well as into the mature NarS-S species. Notably, the UUAUU or UCAUUC sequences around the two NarS processing sites match the minimal RNase E site consensus RN↓WUU (28). Changing the lower NarS processing site from UCAUUC to UCACAG by a silent mutation with respect to the NarK amino acid sequence specifically abolished the processing of NarS-L into NarS-S (Figure 3C, lane 5, P_{narK}-*narK*-$NarS^{UUC\text{-}CAG}$),

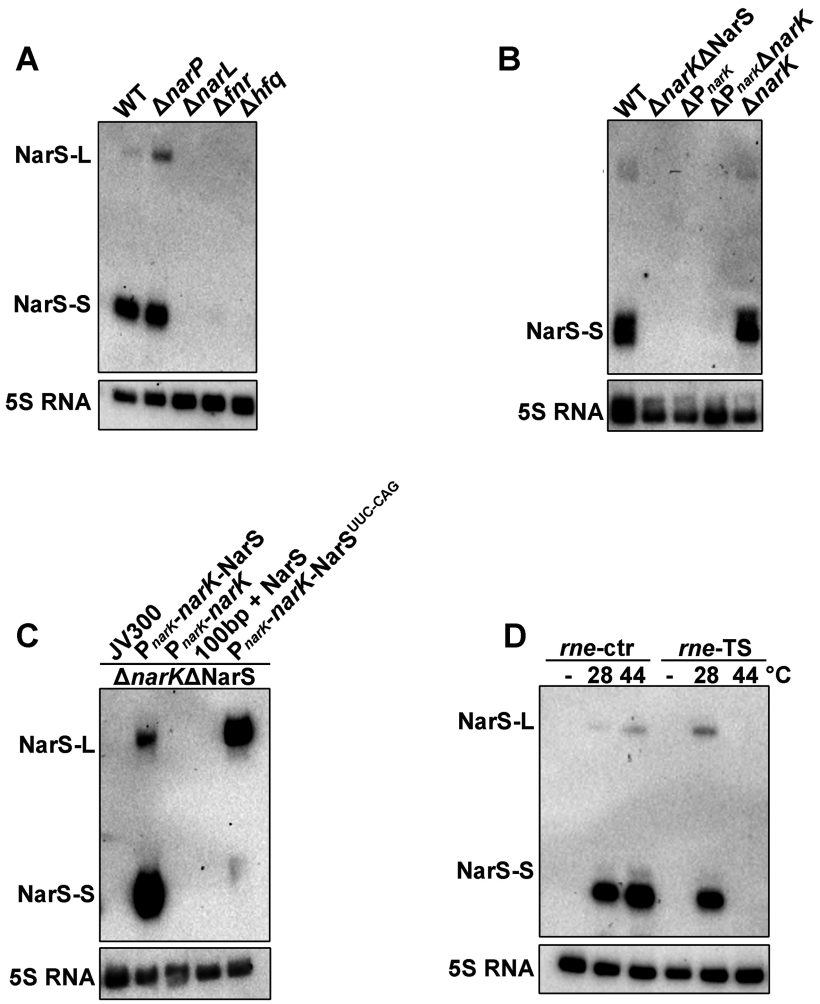

Figure 3. NarS is an Hfq-dependent sRNA processed by RNase E. (**A**) Expression of NarS requires the transcriptional regulators NarL and FNR, and the RBP Hfq. Total RNA was isolated from the indicated strains and analyzed by northern blotting. (**B**) Expression of NarS in *Salmonella* lacking different *narK* regions. Δ*narK*ΔNarS: deletion from *narK* promoter to terminator; ΔP_{narK}, deletion of the *narK* promoter region and retained the whole ORF; ΔP_{nark} Δ*narK*: deletion from *narK* promoter to 100 nt upstream of NarS-S 5′ end; Δ*narK*: deletion from *narK* transcriptional start site to 100 nt upstream of NarS-S 5′ end, while retained the promoter of *narK*. NarS was only detected in this strain. (**C**) Expression of NarS from pZE12-based plasmids carrying different *narK* genomic regions. P_{narK}-*narK*-NarS: plasmid carrying native *narK* promoter and the whole *narK* transcript include the 3′ UTR; P_{narK}-*narK*: plasmid carrying native *narK* promoter and *narK* ORF without the 3′ UTR; 100 bp + NarS: plasmid carrying NarS-S plus upstream 100 bp regions. P_{narK}-*narK*-$NarS^{UUC\text{-}CAG}$: same as P_{narK}-*narK*-NarS but with mutations around NarS-S 5′ end, to mutate the RNase E-recognition motif. (**D**) Northern blot analysis of NarS expression in the RNase E temperature sensitive strain *rne-3071* (*rne*-TS) and the wild-type allele (*rne*-ctr). Bacterial cells were subjected to anaerobic shock after aerobic growth to an OD_{600} of 0.3. '–' indicates RNA samples before anaerobic shock and temperature shift.

pinpointing the specific RNase E cleavage that generates the mature NarS sRNA.

NarS inhibits expression of the nitrite transporter NirC

In pursuit of a biological role of NarS and how it would relate to NarK, we sought to determine potential target mRNAs of NarS under anaerobic conditions. To this end, we compared gene expression in NarS-deficient and NarS overexpression (from plasmid pP_L-NarS) strains following a 30-min anaerobic shock. RNA-seq followed by independent RT-qPCR validation revealed NarS-dependent downregulation of the *nirC* gene, which encodes a conserved nitrite importer (43-fold repression, Figure 4A and Supplementary Table S5). We also detected many other genes with repressed or induced expression upon NarS overexpression (Supplementary Table S5). However, only two of them showed elevated expression in the NarS-deficient strains compared to WT (4.1 ± 1.5-fold for *nirC* and 4.0±1.7-fold for *glnQ,* Figure S6), indicating *nirC* and *glnQ* may be the primary NarS targets under anaerobic growth conditions. Since *glnQ* encodes a subunit of the glutamine ABC transporter, which is not involved in nitrate respiration, we focused our target validation on *nirC*.

To test whether NarS affected the levels of the NirC protein, we added a C-terminal 3xFLAG tag to the chromosomal *nirC* gene. During anaerobic shock, i.e. when NarS levels are high, we observed ∼1.4-fold more NirC protein in ΔNarS compared to the wild-type strain (Figure 4B). This regulation can be ascribed to NarS as there was no

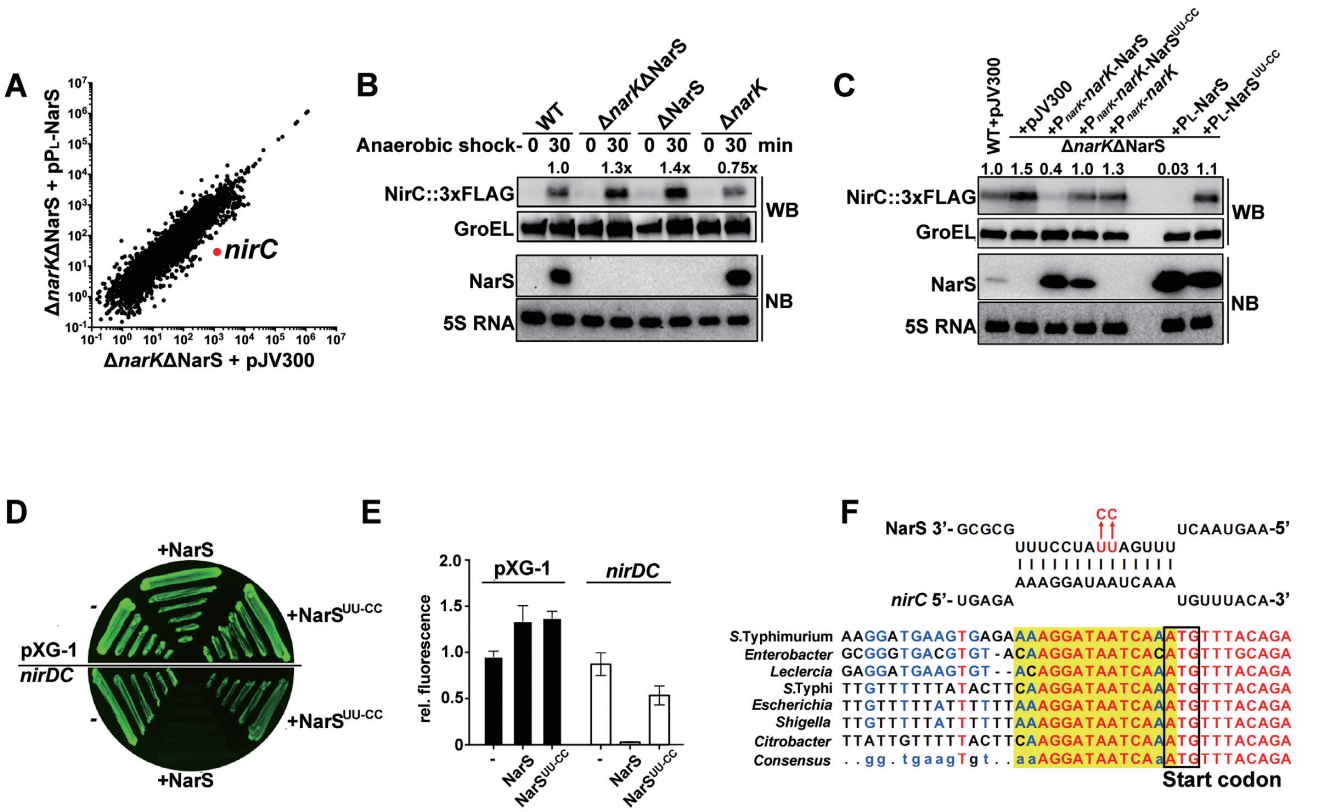

Figure 4. NarS represses expression of the nitrite transporter NirC. (**A**) RNA-seq based comparison of genome-wide mRNA expression (FPKM values) between NarS deleted (Δ*narK*ΔNarS + pJV300) and overexpression (Δ*narK*ΔNarS + pP_L-NarS) strains. Bacteria were subjected to anaerobic shock for 30 min at OD_{600} of 0.3. (**B**) Western and northern blot analyses of NirC::3xFLAG protein and NarS RNA levels, respectively, in different mutant strains. Protein and RNA samples were collected at 0 and 30 min after anaerobic shock at OD_{600} of 0.3. GroEL and 5S rRNA were loading controls. Relative fold changes to wild-type strain are marked above. (**C**) Regulation of the NirC::FLAG protein by ectopically expressed NarS from high-copy plasmids that carry different regions of *nark*-NarS locus. Only strains with a wild-type NarS seed sequence showed reduced NirC expression (lane 3, P_{nark}-*narK*-NarS and line 6, P_L-NarS). Relative fold changes to wild-type strain are marked above. (**D**) Colony fluorescence of Δ*narK*ΔNarS strain carrying either control plasmid pXG-1 (upper) or pXG30-sfGFP in-frame fused with *nirD-nirC* intergenic region (lower), combined with pZE12 based plasmids expressing empty, wild type or mutant NarS. Fluorescence was quantified by FACS and normalized to strain with pJV300 plasmid as shown in (**E**), data represent three independent experiments (mean ± SD). (**F**) Interaction between NarS and *nirC* 5′ UTR mRNA predicated by IntaRNA (upper panel) and conservation of *nirC* Shine-Dalgarno region among of selected enterobacterial genera (lower panel). Conserved nucleotides are marked in red. The base pairing region is highlighted in yellow. The *nirC* start codon is boxed.

further derepression in a Δ*narK*ΔNarS strain, nor did NirC levels increase when the *narK* ORF was disrupted. Thus, the NarK protein itself has no role in NirC expression. This was corroborated by genetic complementation of the Δ*narK*ΔNarS strain. Figure 4C shows that NirC levels decreased by ∼2.5-fold when the full-length *narK*-NarS transcript was expressed from a high-copy plasmid (lane 3, P_{narK}-*narK*-NarS), while overexpression of NarS alone almost fully depleted NirC (lane 6, P_L-NarS). By contrast, overexpression of the NarK protein or a NarS variant with point mutations in the putative seed region ($U_{26}U_{27}$→$C_{26}C_{27}$; details in the next section) had little effect on NirC levels. To conclude, the mRNA of a nitrate transporter makes an sRNA (NarS) that can downregulate the expression of a physiologically related transporter (NirC) under anaerobic conditions.

Evidence for a NarS-*nirC* mRNA interaction

The inhibition of NirC synthesis indicated that NarS acted at the post-transcriptional level. To validate this, we used an established two-plasmid reporter system (36,59) in which NarS is expressed from a constitutive $P_{LlacO-1}$ promoter on one plasmid (pP_L-NarS) and NirC is constitutively expressed as a sfGFP-fusion protein from another plasmid. While NarS had no effect on the GFP control in plasmid pXG-1 (Figure 4D), it strongly repressed the *nirC*-sfGFP fusion (–30.21 ± 0.48-fold, Figure 4E).

Intriguingly, *nirC* also ranked amongst the top target candidates when NarS was queried against enterobacterial mRNAs with the CopraRNA algorithm (60,61). According to this *in silico* prediction, NarS sequesters the Shine-Dalgarno (SD) sequence of *nirC*, forming a perfect 14 bp RNA duplex (Figure 4F) that should be stable enough (62) to inhibit 30S ribosome binding. Not only does the predicted sRNA-mRNA duplex involve the conserved putative seed of NarS, the predicted NarS site in *nirC* is also conserved (Figure 4F), suggesting coevolution of this sRNA-mRNA pair. Furthermore, the *nirC*-NarS pairing is supported by recent RIL-seq data for RNA pairs on Hfq in *E. coli* (9). The seed mutant ($U_{26}U_{27}$→$C_{26}C_{27}$) of NarS no longer represses the *nirC::sfGFP* fusion (Figure

4D–F). Both its detection by RIL-seq and the strong conservation of the interacting bases indicated that the NarS-*nirC* interaction is physiologically relevant.

The NarS-*nirC* RNA duplex was further supported by *in vitro* RNA structure probing (Supplementary Figure S7). Here, we co-incubated *in vitro*-transcribed NarS and *nirC* RNA fragments for 10 min at 37°C, followed by treatment with the ssRNA-specific reagents RNase T1 and lead (II) acetate. RNase T1 cleavage patterns of radiolabelled *nirC* fragments revealed NarS-dependent reduction of cleavage in the –12 nt to +1 nt region of the mRNA (Supplementary Figure S7A and C). This 'footprint' was even more pronounced with lead (II), supporting the predicted base pairing of NarS with the SD region of *nirC*. Reciprocally, the predicted seed of NarS (nucleotides 21–33 of NarS-S) was protected by *nirC* (Supplementary Figure S7B). Additional cleavages were seen in an internal stem of *nirC* mRNA (–25 to –17 nt and +12 to +19 nt regions), and in the NarS terminator (+24 to +32 nt and +39 to +52 nt regions, Supplementary Figure S7C). The unfolding of the internal stem near the *nirC* RBS may contribute to regulation. Thus, NarS through its conserved seed sequesters a conserved 5′ region in *nirC* that is crucial for translation initiation.

Collaborative functions of NarK and NarS in homeostasis of cytoplasmic nitrite

Both the parent and target of NarS are involved in nitrate respiration, prompting us to investigate a potential role of NarS in anaerobic respiration. During anaerobic growth, nitrate is imported by NarK or NarU, and serves as a terminal electron acceptor for anaerobic respiration leading to the production of nitrite (63,64). However, excessive nitrite must be reduced to ammonia or exported to the extracellular space where it may get reimported by NirC (43). Of note, both the *narK* and *nirC* genes are activated by the same transcription factors, FNR and phosphorylated NarL (55,65,66). This simultaneous activation presents a potential intrinsic conflict between nitrite export and accumulation.

To investigate whether NarS controls nitrite accumulation and reduction, we monitored the concentration of nitrite in growth medium as a readout for the rate of nitrate metabolism. Nitrate is imported and converted to nitrite that is then exported primarily via NarK (43). The extracellular concentration of nitrite exported by NarK was analyzed using a chemical assay, using a Δ*narU* strain to eliminate exporter redundancy. When nitrate was supplied to a high concentration (20 mM) in M9CA medium, extracellular nitrite rapidly accumulated after anaerobic shock (Figure 5). As expected, strains lacking NarK (Δ*narK*-Δ*narU* and Δ*narK*ΔNarS-Δ*narU*) are defective in nitrite metabolism and produce ∼3–4-fold (4.018 ± 0.843-fold for Δ*narK*ΔNarS-Δ*narU*; 3.331 ± 1.347-fold for Δ*narK*-Δ*narU*, $P < 0.001$) less nitrite than the parental Δ*narU* strain 45 min into the anaerobic shock. Strikingly, a deletion of NarS markedly reduced the level of extracellular nitrite to nearly half (1.628 ± 0.169-fold, $P < 0.01$) at 45 min after anaerobic shock (ΔNarS-Δ*narU*). The effect was strongest in the transition phase from aerobic to anaerobic growth, with the level of nitrite in the NarS-deficient strain gradually returning to wild-type levels 60 min after cells entered anaerobic growth. Thus, NarS regulates changes in nutrient supply as here shown for the early phase of nitrate respiration.

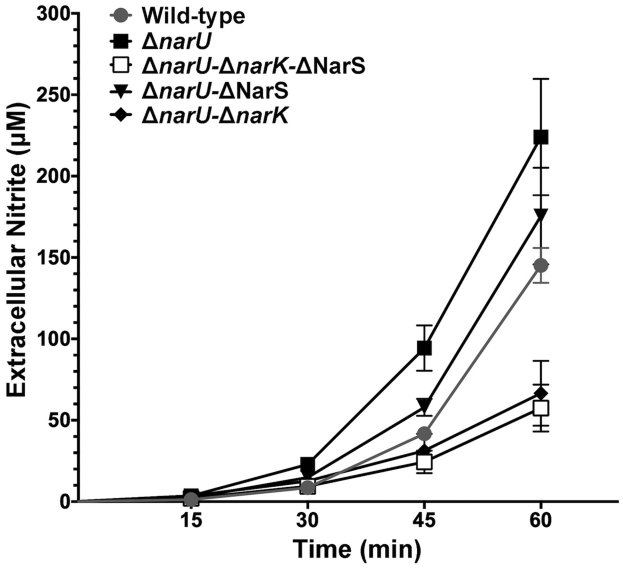

Figure 5. Extracellular nitrite concentrations in anaerobic growth media. Bacterial cells were grown in M9CA medium to OD600 of 0.3 and then supplemented with sodium nitrate (final concentration at 20 mM). Cultures were transferred into 15 ml closed Falcon tubes and incubated without agitation. Samples were collected at 0, 15, 30, 45 and 60 min after anaerobic shock. Supernatants were analyzed to determine nitrite concentration using a colorimetric assay as described in materials and methods.

NarS mediates discoordinate regulation of the *nirBDC-cysG* operon

The NarS target *nirC* is the third gene in the *nirBDC-cysG* operon (Figure 6A) (65). Within this operon, *nirB* and *nirD* encode a nitrite reductase complex that reduces nitrite to ammonia. The downstream gene *cysG* encodes an essential protein to make the siroheme prosthetic group of NirB but also of sulphite reductase, which is required during aerobic growth (67,68). This argued that *cysG* must in part be expressed independently of *nirBD*. Nonetheless, the related functions of these genes in nitrate respiration raised the question of their potential corepression with *nirC*. To address this, we constructed nonpolar chromosomal 3xFLAG fusions for NirB, NirD and CysG, and examined their mRNA and protein levels upon deletion and overexpression of NarS. Surprisingly, none of the three proteins showed regulation by NarS (Figure 6B). On the RNA level, where overexpressed NarS strongly reduced the *nirC* mRNA (∼71-fold down; Supplementary Figure S8), the downstream *cysG* mRNA was reduced by only ∼3.2 ± 0.94-fold, and there was negligible regulation of the upstream *nirB* and *nirD* mRNAs. Thus, unlike many other sRNAs, NarS specifically repressed an internal gene (*nirC*), uncoupling its expression from the rest of the *nirBDC-cysG* operon.

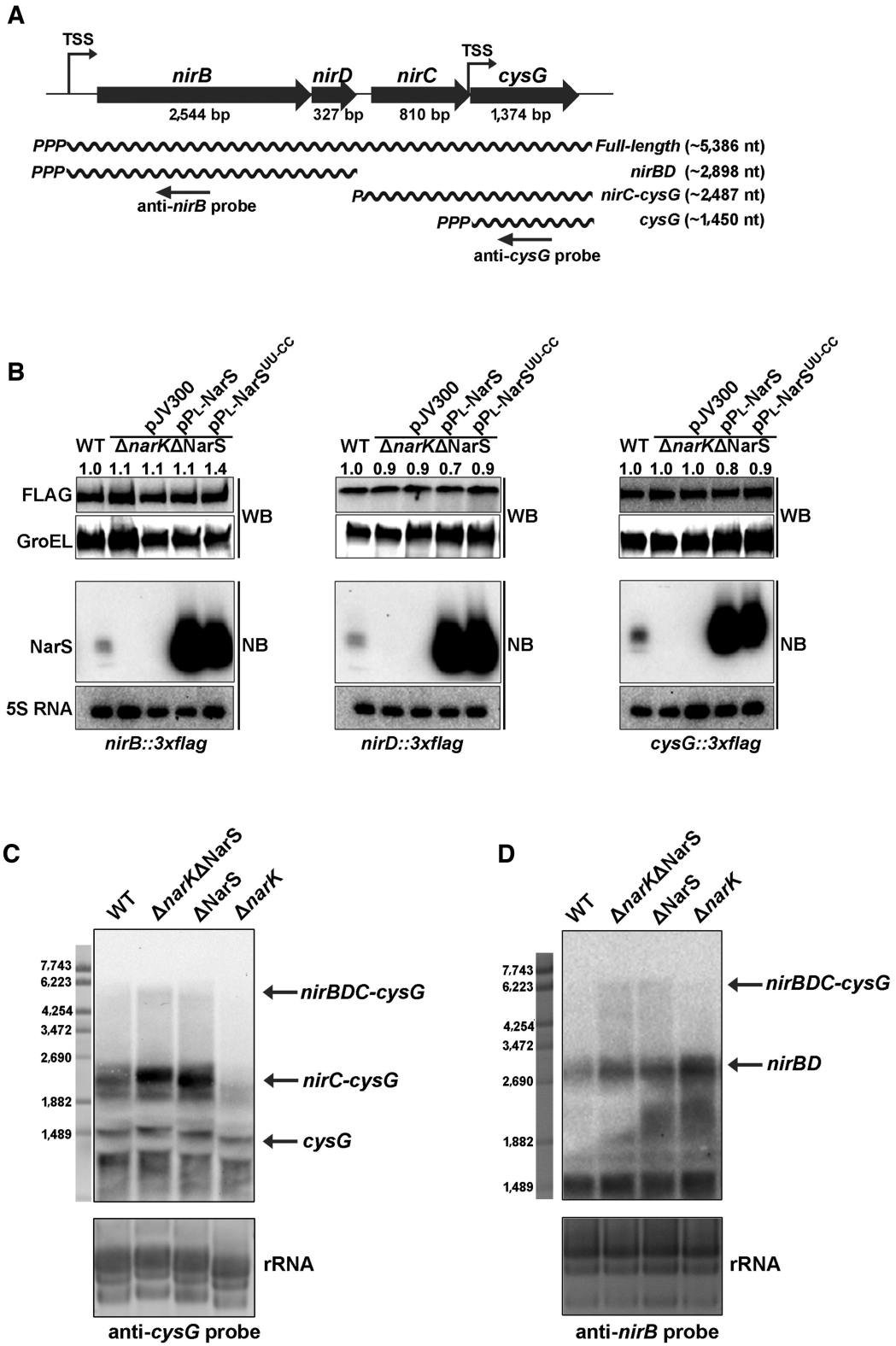

Figure 6. NarS selectively regulates the expression of *nirC* mRNA within the *nirBDC-cysG* operon. (**A**) Genomic organization of the *nirBDC-cysG* operon. Northern blot detection of mRNA isoforms and their predicted length are shown below. 'PPP' refers to a tri-phosphorylated 5′ end and 'P' refers to a mono-phosphorylated 5′ end, as determined by 5′ RACE. (**B**) Analyses of NirB::FLAG, NirD::FLAG and CysG::FLAG proteins and NarS RNA levels in individually Flag-tagged strains. Wild-type or mutant NarS were constitutively expressed from high-copy plasmids (pP_L-NarS). Relative fold changes to wild-type strain are marked above. (**C, D**) Northern blot analyses of *nirBDC-cysG* mRNA expression. Total RNA was collected from anaerobic shock treated cells and separated by 1.2% agrose gel. λ-EcoT14 I/Bgl II digest was loaded as marker and rRNA was visualized by EtBr staining before transferring to membrane. Multiple bands were detected by the anti-*cysG* (C) and anti-*nirB* (D) probes, as marked by arrows. The reduced levels of *nirC-cysG* in Δ*narK* was due to altered NarS expression in this strain.

Suboperon structures of the *nirBDC-cysG* transcript

If NarS does not affect the downstream *cysG* gene, one possibility is that *nirC* and *cysG* are transcribed separately. To address this, we examined northern blot signals of *nirBDC-cysG* from anaerobic-shock cells, probing for either *cysG* or the *nirBD* region. As shown in Figure 6C (lane WT), a weak band of 5.4 kb that likely is the full-length *nirBDC-cysG* mRNA was detected by both RNA probes, arguing that *nirBDC-cysG* is indeed transcribed as a polycistronic mRNA. In addition, two stronger *cysG*-specific bands (1.4 kb and 2.5 kb) were detected (Figure 6C, lane WT), as well as a 2.8 kb band specific to the *nirB* probe (Figure 6D, lane WT). Judging from the gene size, these three bands should correspond to *cysG*, *nirC-cysG*, and *nirBD* mRNA fragments (Figure 6A). In other words, an intricate suboperonic structure may explain why *cysG* is refractory to NarS.

To better characterize these fragments, we performed RACE to identify the 5′ ends for each gene in the *nirBDC-cysG* operon. The 5′ end of *nirB* perfectly matched the TSS of *nirBDC-cysG* as annotated by dRNA-seq (Supplementary Figure S9) (32). We failed to detect a primary 5′ end for *nirD*, supporting the northern blot interpretation that *nirD* is co-transcribed with *nirB*. Interestingly, multiple 5′ ends were detected for *nirC*, all of which are located in a uridine-rich region starting at the *nirD* stop codon (Supplementary Figure S9), as if the *nirC* mRNA accumulated independently as a processed fragment of the long *nirBDC-cysG* transcript. Processing at this site would generate a *nirBD* fragment (∼2.8 kb) and a *nirC-cysG* fragment (∼2.5 kb), both observed on the northern blot (Figure 6C-D). Finally, a prominent 5′ end was detected for the terminal *cysG* gene, suggesting that as in *E. coli* (69), *Salmonella cysG* is independently transcribed from an extended -10 promoter (70). This promoter would yield a ∼1.4 kb transcript, matching the shorter of the two *cysG* bands seen on the northern blots. We conclude that the *nirBDC-cysG* operon is transcribed from two independent promoters producing two primary transcripts: a *cysG* mRNA, and a full *nirBDC-cysG* mRNA that is further processed into *nirBD* and *nirC-cysG* fragments (Figure 6A).

NarS selectively promotes the degradation of *nirC*-containing mRNA

Having established the individual transcripts in the *nirBDC-cysG* operon, we next sought to examine their regulation in strains lacking *narK*, NarS or both. Strikingly, NarS deletion caused strong accumulation of the *nirC-cysG* fragment (Δ*narK*ΔNarS and ΔNarS), and a moderate upregulation of the full-length *nirBDC-cysG* transcript (ΔNarS), indicating that NarS targets both *nirC-cysG* and the parental *nirBDC-cysG* transcript (Figure 6C). However, NarS is not required for *nirBDC-cysG* processing, since the *nirBD* and *nirC-cysG* forms are also detected in the absence of NarS (Figure 6C and D). Thus, the processed *nirC-cysG* fragment is the primary target of NarS, with the *nirBDC-cysG* polycistronic mRNA being a secondary target.

Intra-operonic terminator is required for NarS-selective regulation

We considered it likely that processing of the *nirC-cysG* fragment, the primary target of NarS, involves RNase E because the 5′ ends mapped in the uridine track at the *nirD* stop codon (Figure 7A) resembled a candidate region for RNase E cleavage (28). Indeed, inactivation of RNase E reduced *nirC-cysG* transcript levels while the full-length *nirBDC-cysG* mRNA accumulated (Figure 7B). After processing the full-length mRNA to generate a stable *nirC-cysG* transcript that is then subject to regulation by NarS, RNase E may continue to degrade the 5′ half (*nirBD*) of the polycistronic mRNA (Figure 7C). Despite its rapid degradation, the *nirBD* fragment is still detectable in WT cells (Figure 6D), indicating a mechanism that protects its vulnerable 3′ ends against exoribonucleases. Inspection of the *nirBD* 3′ ends revealed a stem-loop structure (ΔG –14.90 kcal/mol) followed by a uridine track, resembling an intrinsic terminator (Figure 7A). This intra-operonic terminator may stabilize the cleaved *nirBD* fragments, but may also promote premature transcription termination/attenuation that generates similar *nirBD* transcripts.

To dissect the roles of this putative operon-internal terminator, we tested how transcript patterns changed upon its deletion (ΔsU). This was done in a NarS-deficient background to exclude NarS effects on the full-length operon and shorter *nirC-cysG* transcripts. Indeed, mutation of the terminator caused a reduction of the *nirBD* transcripts (Figure 7D). Concomitantly, the level of the *nirC-cysG* transcript increased (Figure 7E, compare lanes 1 and 3). Without internal termination, read-through of full-length transcript may occur, possibly yielding more precursor of the *nirC-cysG* transcript. Intriguingly, we observed that the 5′ ends of the resulting *nirC-cysG* transcripts shifted to around the TTAATT stop codon region of *nirD* (Figure 7A).

The above results suggested that an intra-operonic terminator acted as a *cis*-encoded repressor of *nirC-cysG* expression, in addition to the *trans*-encoded repressor NarS. Most surprisingly, we observed that this *cis*-encoded repressor was also essential for the NarS-mediated regulation of *nirC* in *trans*. This is to say that removal of the intra-operonic terminator abrogated the NarS-induced degradation of the *nirC-cysG* mRNA (Figure 7E, compare lanes 2 and 4), despite the fact that the NarS site in *nirC* is located ∼200 nt downstream of the uridine track. This was further confirmed at the protein level by deleting the same region in the *nirDC-sfGFP* reporter. Figure 7F-G shows that the NarS-mediated repression drops from ∼30-fold to ∼5-fold upon terminator deletion. A possible explanation for this effect is that the uridine stretch may be an Hfq binding site in the mRNA, as the *nirBD* transcript appears to be stabilized by Hfq (Supplementary Figure S10). Loss of Hfq binding site its 5′ region would prevent *nirC* from being stably recognized by NarS. Taken together, these data suggest that the post-processing of the *nirBDC-cysG* operon mRNA is highly coordinated by RNase E cleavage, intrinsic transcriptional termination, and base pairing by NarS.

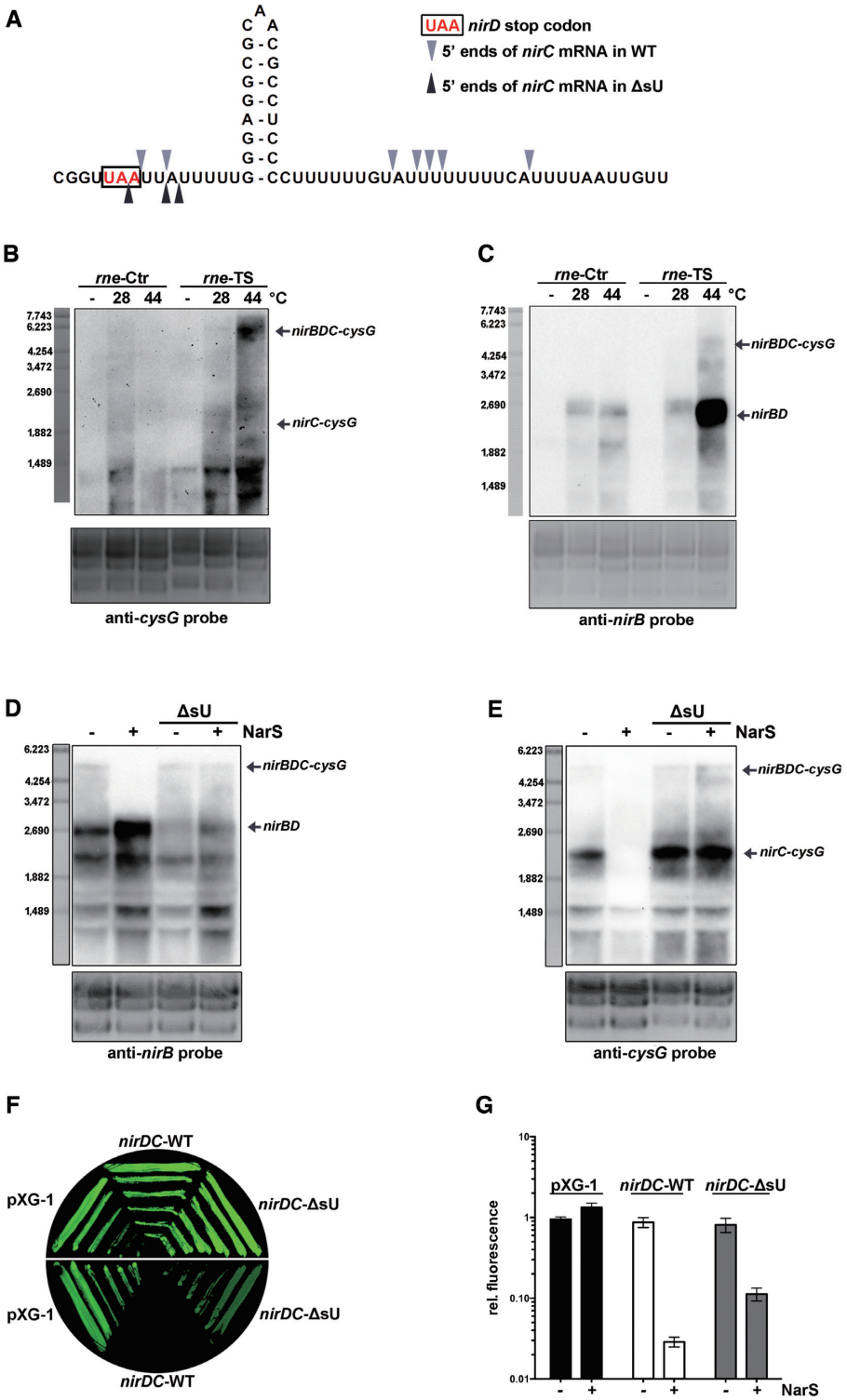

Figure 7. An intergenic terminator is required for selective regulation by NarS. (**A**) Genomic context of the putative terminator downstream of *nirD*. Arrows refer to the 5′ ends of *nirC* mRNA as detected by 5′ RACE. (**B, C**) Expression of *nirBDC-cysG* and different isoforms in the RNase E temperature sensitive strain. Bacteria were grown to OD_{600} of 0.3, filled into 50 ml closed Falcon tubes and incubated without agitation at 28°C or 44°C for 30 min. '–' indicates RNA samples before anaerobic shock and temperature shift. Total RNA was separated on a 1.2% agarose gel for northern blotting analysis. λ-EcoT14 I/Bgl II digest was loaded as marker and rRNA was visualized by ethidium bromide staining before transfer to membrane. (**D, E**) Expression of *nirBDC-cysG* and different isoforms in *nirD* terminator and U-track deleted strain (ΔsU) in the presence and absence of NarS. (**F, G**) Fluorescence of Δ*narK*ΔNarS strain carrying either control plasmid pXG-1 (control), or pXG30-sfGFP in-frame fused with wild-type (*nirDC*-WT) or ΔsU (*nirDC*-ΔsU) *nirD-nirC* intergenic region combined with empty vector pJV300 (upper half) or NarS expressing plasmid (pP_L-NarS) (lower half). Fluorescence was quantified in a strain carrying pZE12 empty vector (upper half) or pZE12 expressing NarS (upper half). Fluorescence was normalized to a strain with control plasmid pJV300. Data represent three independent experiments (mean ± SD).

DISCUSSION

In this study, we have identified NarS as a new 3′ UTR-derived sRNA in the nitrate metabolism pathway. We propose that this low-confidence candidate is a physiologically relevant riboregulator that represses the synthesis of one nitrite transporter in order to balance its expression with that of another metabolically related transporter. Interestingly, the NarS-mediated mRNA crosstalk discovered here in enterobacteria echoes the pioneering findings on mRNA crossregulation of superoxide dismutases in actinobacteria (21) such that in both cases the 3′ UTR-derived sRNA helps to resolve an intrinsic conflict in the same metabolic pathway. Currently, there are too few well-characterized such sRNAs to allow for generalization, but we consider it likely that such mRNA-mediated fine-tuning within metabolic pathways is a major functional theme in enterobacteria because they encounter many different metabolic niches inside and outside their hosts. Moreover, NarS, as judged by the conserved seed region, is restricted to a sub-clade of *Enterobacteriaceae* that is dominated by animal-associated members, i.e. *Salmonella*, *Escherichia*, *Shigella*, *Cronobacter* and *Cedecea* (Supplementary Figure S1). By contrast, NarS seems to be absent from the plant-associated clade, which includes *Dickeya*, *Pectobacterium*, and *Pantoea* bacteria. This suggests that the emergence of NarS-mediated mRNA crosstalk coincided with the separation between animal and plant enterobacteria, perhaps to facilitate adaption to an animal host-associated lifestyle.

Solving metabolic conflicts by a 3′ UTR-derived sRNA

Intestinal pathogens such as *Salmonella* catalyze a short-circuit of nitrate metabolism from nitrate to ammonia via nitrite (71). This two-step anaerobic reduction process provides abundant electrons for bacteria in environments with limited oxygen such as the human gastrointestinal tract (72). *Salmonella* encode both cytoplasmic and periplasmic reductases to catalyze the reduction from nitrate to ammonia (73). The cytoplasmic pathway comprises nitrate reductase NarA (encoded by *narGHIJ* or *narUZYWV*) and nitrite reductase NirBD (encoded by *nirBDC-cysG*). Unlike NarA that requires nitrate/nitrite exchangers NarK or NarU to transport the negatively charged nitrate anion into cytoplasm for reduction, substrates of NirBD reductase can be taken up by NirC from extracellular or periplasmic nitrite, or be directly generated during cytoplasmic nitrate reduction. Switching between these two pathways is important for bacteria to adapt to different concentrations of environmental nitrate or nitrite.

When extracellular concentration of nitrate is low or nitrite is abundant, the two-component regulatory system NarX/P will activate the *nirBDC-cysG* operon (53), and nitrite will be imported into the cytoplasm by NirC and reduced by NirBD to provide electrons for anaerobic respiration. In this case, the functions of NirBD and NirC from the same operon are coordinated. By contrast, when environmental nitrate is sufficient to activate the NarQ/L system, phosphorylated NarL will induce expression of *narK*, *narGHI* and *nirBDC-cysG* simultaneously (54,74,75), therefore the NarK protein will both import extracellular nitrate for NarA(NarGHI)-dependent nitrate reduction and export the product nitrite. In this case, nitrate reduction is enough to provide electrons for anaerobic respiration and accumulation of nitrite product would be toxic. NirBD then reduces cytoplasmic nitrite to ammonia for detoxification. However, the *nirBDC-cysG* operon encodes both a nitrite reductase and a nitrite transporter with potentially conflicting roles in controlling intracellular nitrite homeostasis (65). Our work suggests a model (Figure 8) whereby the co-activation of *narK* with the *nirB* operon serves a dual purpose in resolving this conflict: the *narK*-derived sRNA NarS prevents expression of the nitrite importer NirC to limit uptake of excessive nitrite in the environment, while maintaining the synthesis of NirBD and reduction of intracellular nitrite to ammonia. Thus, the crosstalk between the *narK* and *nirC* mRNAs balances extracellular (or periplasmic) and cytoplasmic substrates for NirBD reductase.

Interestingly, other noncoding regulators related to nitrate, all of which of intergenic origin, have recently been discovered. These include the NsiR4 sRNA in *Synechocystis* (76), the NfiS sRNA in root-associated bacterium *Pseudomonas stutzeri* (77), and the RpoS-dependent SdsN sRNA that represses the nitroreductase NfsA and NO dioxygenase HmpA in *E. coli* (78). However, whereas these sRNAs mainly act to regulate nitrate assimilation, NarS targets respiratory reduction of nitrate, which is critical for the survival of facultative anaerobic bacteria in electron-rich environments such as the human gastrointestinal tract. Unsurprisingly, anaerobic metabolism is regulated by additional sRNAs, for example, the conserved enterobacterial FnrS sRNAs that endows the transcriptional regulator FNR with an mRNA repressor arm (79).

3′ UTR-derived sRNAs and RNase E

NarS is a new member of a growing list of so-called type II sRNAs from mRNA 3′ regions (2). Different from the type I sRNAs that are transcribed from ORF-internal promoters, the production of type II sRNAs is intimately coupled to their parental mRNAs from which they are released by endonucleolytic processing, as shown for CpxQ, GadF, RaiZ, SdhX and SroC (3,6–9,23). Such sRNA biogenesis pathways might provide an economic way of evolving an extra gene function for an mRNA. It currently remains unclear how many mRNAs of a given bacterium yield such additional sRNA regulators. Considering *Salmonella*, Hfq CLIP-seq has captured ∼120 peaks from 3′ UTR of coding genes (44) and many of these regions possess RNase E sites around their stop codon (28). However, only 21 Hfq-bound sRNA are presently annotated as 3′ UTR-derived sRNAs. It is reasonable to believe that the actual number of mRNA 3′ ends with independent functions is higher, because even obvious candidates such as the 3′ UTRs of *acnB*, *mltA* and *sodA* are not included yet. A likely explanation for the incomplete annotation is the low expression of these 3′ UTR-derived sRNAs under standard growth in LB-broth. Global RNA interactome mapping by RIL-seq (9) or CLASH (80), performed for both Hfq and ProQ, and

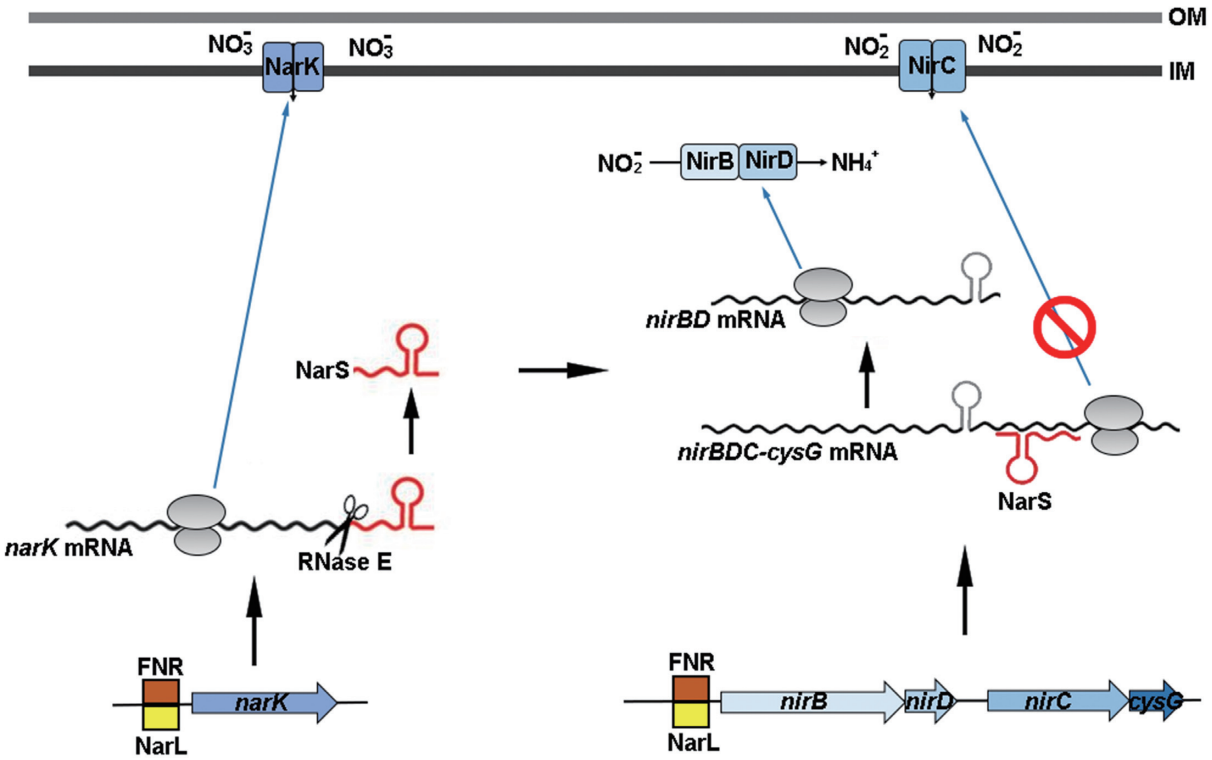

Figure 8. Coordinated regulation of nitrate metabolism by NarK and the 3′ UTR sRNA NarS. Under anaerobic conditions with abundant nitrate, transcriptional regulators FNR and NarL activate the transcription of nitrate/nitrite antiporter NarK, respiratory nitrate reductase *narGHI* and operon *nirBDC-cysG*. Nitrate is imported by NarK into the bacterial cytoplasm where it is reduced to nitrite by the respiratory nitrate reductase NarG. To protect the cytoplasm from excess nitrite toxicity, reductase NirBD catalyzes subsequent reduction of nitrite to ammonia. NarS is processed from the *narK* mRNA by RNase E to repress the expression of nitrite transporter NirC to limit nitrite import.

in a variety of non-standard growth conditions, could be a straightforward path to obtaining an approximation of the full scope of mRNA crosstalk in *E. coli* and *Salmonella*.

Discoordinate regulation of operons by sRNAs

Despite sharing the same transcript, cistrons in bacterial operons often show discoordinate expression in response to regulatory signals (81,82). Suboperonic regulation at the transcriptional level can result from secondary promoters, a scenario found here with the internal *cysG* promoter within the *nirBDC-cysG* operon. The shorter *cysG* transcript escapes NarS-mediated regulation which makes sense because the CysG protein converts uroporphyrinogen III into siroheme (67,83), the latter of which is needed for reducing the nitrite production.

Suboperonic regulation can also occur on the post-transcriptional level by cistron-specific targeting by sRNAs (37,84). One interesting case is the *iscRSUA* mRNA in *E. coli* (85) in which RyhB sRNA represses translation initiation of *iscS*, which triggers RNA degradation of the downstream *iscSUA* cistrons, but also stabilizes the upstream *iscR* cistron that carries a repetitive extragenic palindromic (REP) RNA secondary structure at its 3′ end. There is some parallel with the *nirBDC-cysG* regulation by NarS: base pairing in the middle of an operon mRNA promotes downstream decay but also stabilizes the upstream fragments. The difference is the use of a REP element versus a transcription terminator, with terminators being more widely used for setting differential expression of operonic genes in divergent bacteria (86). Again, RIL-seq studies under various growth conditions should be informative as to whether 3′ UTR-derived sRNAs are used predominantly for either simple schemes of mRNA antagonism or more complex regulation of polycistronic operon mRNAs similar to the *nirBDC-cysG* case reported here.

The uridine-rich region following the internal *nirD* terminator has two different functions. First, it stops transcription. Second, by a molecular mechanism yet to be established it also enables NarS-mediated regulation of *nirC*, although the NarS site is ∼200 nt away. One possible explanation is that these uridines provide an Hfq binding site necessary to anneal NarS to this target. No peaks were detected from *nirD-nirC* intergenic region in Hfq-CLIP data, but this could be due to the marginal expression of *nirBDC-cysG* during aerobic growth. However, Hfq-CLIP showed a generally strong enrichment of binding at Rho-independent terminators followed by a U-rich sequence (44), making the *nirD* terminator a likely candidate. Since targets of Hfq-dependent sRNAs usually require a binding site for the distal side of Hfq (87), deletion of the U-track in upstream of the *nirC* mRNA might prevent RNA duplex formation and regulation.

When RNase E was inactivated, the *nirC-cysG* isoform disappeared, at the same time, the full-length operon

mRNA accumulated. Although the evidence is indirect, RNase E is likely the responsible nuclease in processing the full transcript. The processing is independent of NarS, suggesting that the full-length *nirBDC-cysG* mRNA is pre-processed into *nirBD* and *nirC-cysG* by RNase E as well. This is similar to the discoordinate expression of the polycistronic *glmUS* mRNA in *E. coli* which is also processed by RNase E before the GlmZ sRNA targets it for further regulation (88–90). In the present case, we speculate that the long untranslated, ribosome-free region between *nirD* and *nirC* offers an opportunity for RNase E to attack in its 5′-end-independent direct access mode (91,92), before it processes the mRNA further around the *nirD* stop codon.

In conclusion, the present study of NarS has revealed a complex pattern of post-transcriptional *cis* and *trans* regulations in mRNAs with important metabolic functions in a model Gram-negative bacterium. Gram-positive bacteria use a different set of nucleases to process their transcripts (93). As the first functional 3′ UTR-derived sRNAs are getting characterized in those species (94), it will be interesting to see how the mechanisms of mRNA crosstalk compare amongst distantly related groups of microbes.

DATA AVAILABILITY

Gene expression data have been deposited with NCBI Gene Expression Omnibus (GEO) under accession number GSE135757.

SUPPLEMENTARY DATA

Supplementary Data are available at NAR Online.

ACKNOWLEDGEMENTS

The authors thank Jeffrey A. Cole, Franziska Faber, Jens Hör and Kai Papenfort for critical reading and editing and for very helpful comments on the manuscript.

FUNDING

National Natural Science Foundation of China [31500053 and 81991532 to C.W.]; Shanghai Municipal Education Commission [15CG03 to C.W.]; DFG, German Research Council [Vo875/14-1 to J.V.]. The open access publication charge for this paper has been waived by Oxford University Press - *NAR* Editorial Board members are entitled to one free paper per year in recognition of their work on behalf of the journal.
Conflict of interest statement. None declared.

REFERENCES

1. Grull,M.P. and Masse,E. (2019) Mimicry, deception and competition: the life of competing endogenous RNAs. *Wiley Interdiscip. Rev. RNA*, **10**, e1525.
2. Miyakoshi,M., Chao,Y. and Vogel,J. (2015) Regulatory small RNAs from the 3′ regions of bacterial mRNAs. *Curr. Opin. Microbiol.*, **24**, 132–139.
3. Chao,Y. and Vogel,J. (2016) A 3′ UTR-Derived small RNA Provides the regulatory noncoding arm of the inner membrane stress response. *Mol. Cell*, **61**, 352–363.
4. Grabowicz,M., Koren,D. and Silhavy,T.J. (2016) The CpxQ sRNA negatively regulates skp to prevent mistargeting of beta-Barrel outer membrane proteins into the cytoplasmic membrane. *MBio*, **7**, e00312-16.
5. Peng,T., Berghoff,B.A., Oh,J.I., Weber,L., Schirmer,J., Schwarz,J., Glaeser,J. and Klug,G. (2016) Regulation of a polyamine transporter by the conserved 3′ UTR-derived sRNA SorX confers resistance to singlet oxygen and organic hydroperoxides in Rhodobacter sphaeroides. *RNA Biol*, **13**, 988–999.
6. Smirnov,A., Wang,C., Drewry,L.L. and Vogel,J. (2017) Molecular mechanism of mRNA repression in trans by a ProQ-dependent small RNA. *EMBO J.*, **36**, 1029–1045.
7. Miyakoshi,M., Matera,G., Maki,K., Sone,Y. and Vogel,J. (2018) Functional expansion of a TCA cycle operon mRNA by a 3′ end-derived small RNA. *Nucleic. Acids. Res.*, **47**, 2075–2088.
8. De Mets,F., Van Melderen,L. and Gottesman,S. (2019) Regulation of acetate metabolism and coordination with the TCA cycle via a processed small RNA. *PNAS*, **116**, 1043–1052.
9. Melamed,S., Peer,A., Faigenbaum-Romm,R., Gatt,Y.E., Reiss,N., Bar,A., Altuvia,Y., Argaman,L. and Margalit,H. (2016) Global mapping of small RNA-target interactions in bacteria. *Mol. Cell*, **63**, 884–897.
10. Holmqvist,E. and Vogel,J. (2018) RNA-binding proteins in bacteria. *Nat. Rev. Microbiol.*, **16**, 601–615.
11. Kavita,K., de Mets,F. and Gottesman,S. (2018) New aspects of RNA-based regulation by Hfq and its partner sRNAs. *Curr. Opin. Microbiol.*, **42**, 53–61.
12. Olejniczak,M. and Storz,G. (2017) ProQ/FinO-domain proteins: another ubiquitous family of RNA matchmakers? *Mol. Microbiol.*, **104**, 905–915.
13. Jagodnik,J., Brosse,A., Le Lam,T.N., Chiaruttini,C. and Guillier,M. (2017) Mechanistic study of base-pairing small regulatory RNAs in bacteria. *Methods*, **117**, 67–76.
14. Vogel,J., Bartels,V., Tang,T.H., Churakov,G., Slagter-Jager,J.G., Huttenhofer,A. and Wagner,E.G. (2003) RNomics in Escherichia coli detects new sRNA species and indicates parallel transcriptional output in bacteria. *Nucleic Acids Res.*, **31**, 6435–6443.
15. Zhang,A., Wassarman,K.M., Rosenow,C., Tjaden,B.C., Storz,G. and Gottesman,S. (2003) Global analysis of small RNA and mRNA targets of Hfq. *Mol. Microbiol.*, **50**, 1111–1124.
16. Kawano,M., Reynolds,A.A., Miranda-Rios,J. and Storz,G. (2005) Detection of 5′- and 3′-UTR-derived small RNAs and cis-encoded antisense RNAs in Escherichia coli. *Nucleic Acids Res.*, **33**, 1040–1050.
17. Chao,Y., Papenfort,K., Reinhardt,R., Sharma,C.M. and Vogel,J. (2012) An atlas of Hfq-bound transcripts reveals 3′ UTRs as a genomic reservoir of regulatory small RNAs. *EMBO J.*, **31**, 4005–4019.
18. Fender,A., Elf,J., Hampel,K., Zimmermann,B. and Wagner,E.G. (2010) RNAs actively cycle on the Sm-like protein Hfq. *Genes Dev.*, **24**, 2621–2626.
19. Gottesman,S. and Storz,G. (2015) RNA reflections: converging on Hfq. *RNA*, **21**, 511–512.
20. Guo,M.S., Updegrove,T.B., Gogol,E.B., Shabalina,S.A., Gross,C.A. and Storz,G. (2014) MicL, a new sigmaE-dependent sRNA, combats envelope stress by repressing synthesis of Lpp, the major outer membrane lipoprotein. *Genes Dev.*, **28**, 1620–1634.
21. Kim,H.M., Shin,J.H., Cho,Y.B. and Roe,J.H. (2014) Inverse regulation of Fe- and Ni-containing SOD genes by a Fur family regulator Nur through small RNA processed from 3′UTR of the sodF mRNA. *Nucleic Acids Res.*, **42**, 2003–2014.
22. Eisenhardt,K.M.H., Reuscher,C.M. and Klug,G. (2018) PcrX, an sRNA derived from the 3′- UTR of the Rhodobacter sphaeroides puf operon modulates expression of puf genes encoding proteins of the bacterial photosynthetic apparatus. *Mol. Microbiol.*, **110**, 325–334.
23. Miyakoshi,M., Chao,Y. and Vogel,J. (2015) Cross talk between ABC transporter mRNAs via a target mRNA-derived sponge of the GcvB small RNA. *EMBO J.*, **34**, 1478–1492.
24. Acuna,L.G., Barros,M.J., Penaloza,D., Rodas,P.I., Paredes-Sabja,D., Fuentes,J.A., Gil,F. and Calderon,I.L. (2016) A feed-forward loop between SroC and MgrR small RNAs modulates the expression of

eptB and the susceptibility to polymyxin B in Salmonella Typhimurium. *Microbiology*, **162**, 1996–2004.
25. Mackie,G.A. (2013) RNase E: at the interface of bacterial RNA processing and decay. *Nat. Rev. Microbiol.*, **11**, 45–57.
26. Mohanty,B.K. and Kushner,S.R. (2016) Regulation of mRNA Decay in bacteria. *Annu. Rev. Microbiol.*, **70**, 25–44.
27. Bandyra,K.J. and Luisi,B.F. (2018) RNase E and the high-fidelity orchestration of RNA metabolism. *Microbiol. Spectr.*, **6**, doi:10.1128/microbiolspec.RWR-0008-2017.
28. Chao,Y., Li,L., Girodat,D., Forstner,K.U., Said,N., Corcoran,C., Smiga,M., Papenfort,K., Reinhardt,R., Wieden,H.J. *et al.* (2017) In Vivo cleavage map illuminates the central role of RNase E in coding and non-coding RNA pathways. *Mol. Cell*, **65**, 39–51.
29. Sauer,E. and Weichenrieder,O. (2011) Structural basis for RNA 3′-end recognition by Hfq. *Proc. Natl. Acad. Sci. U.S.A.*, **108**, 13065–13070.
30. Ishikawa,H., Otaka,H., Maki,K., Morita,T. and Aiba,H. (2012) The functional Hfq-binding module of bacterial sRNAs consists of a double or single hairpin preceded by a U-rich sequence and followed by a 3′ poly(U) tail. *RNA*, **18**, 1062–1074.
31. Holmqvist,E., Li,L., Bischler,T., Barquist,L. and Vogel,J. (2018) Global maps of ProQ binding in vivo reveal target recognition via RNA Structure and stability control at mRNA 3′ Ends. *Mol. Cell*, **70**, 971–982.
32. Kroger,C., Dillon,S.C., Cameron,A.D., Papenfort,K., Sivasankaran,S.K., Hokamp,K., Chao,Y., Sittka,A., Hebrard,M., Handler,K. *et al.* (2012) The transcriptional landscape and small RNAs of Salmonella enterica serovar typhimurium. *Proc. Natl. Acad. Sci. U.S.A.*, **109**, E1277–E1286.
33. Kroger,C., Colgan,A., Srikumar,S., Handler,K., Sivasankaran,S.K., Hammarlof,D.L., Canals,R., Grissom,J.E., Conway,T., Hokamp,K. *et al.* (2013) An infection-relevant transcriptomic compendium for salmonella enterica serovar typhimurium. *Cell Host Microbe*, **14**, 683–695.
34. Datsenko,K.A. and Wanner,B.L. (2000) One-step inactivation of chromosomal genes in Escherichia coli K-12 using PCR products. *PNAS*, **97**, 6640–6645.
35. Uzzau,S., Figueroa-Bossi,N., Rubino,S. and Bossi,L. (2001) Epitope tagging of chromosomal genes in Salmonella. *PNAS*, **98**, 15264–15269.
36. Urban,J.H. and Vogel,J. (2007) Translational control and target recognition by Escherichia coli small RNAs in vivo. *Nucleic Acids Res.*, **35**, 1018–1037.
37. Papenfort,K., Sun,Y., Miyakoshi,M., Vanderpool,C.K. and Vogel,J. (2013) Small RNA-mediated activation of sugar phosphatase mRNA regulates glucose homeostasis. *Cell*, **153**, 426–437.
38. Li,R., Li,Y., Kristiansen,K. and Wang,J. (2008) SOAP: short oligonucleotide alignment program. *Bioinformatics*, **24**, 713–714.
39. Kim,D., Langmead,B. and Salzberg,S.L. (2015) HISAT: a fast spliced aligner with low memory requirements. *Nat. Methods*, **12**, 357–360.
40. Langmead,B. and Salzberg,S.L. (2012) Fast gapped-read alignment with Bowtie 2. *Nat. Methods*, **9**, 357–359.
41. Li,B. and Dewey,C.N. (2011) RSEM: accurate transcript quantification from RNA-Seq data with or without a reference genome. *BMC Bioinformatics*, **12**, 323.
42. Smirnov,A., Forstner,K.U., Holmqvist,E., Otto,A., Gunster,R., Becher,D., Reinhardt,R. and Vogel,J. (2016) Grad-seq guides the discovery of ProQ as a major small RNA-binding protein. *PNAS*, **113**, 11591–11596.
43. Clegg,S., Yu,F., Griffiths,L. and Cole,J.A. (2002) The roles of the polytopic membrane proteins NarK, NarU and NirC in Escherichia coli K-12: two nitrate and three nitrite transporters. *Mol. Microbiol.*, **44**, 143–155.
44. Holmqvist,E., Wright,P.R., Li,L., Bischler,T., Barquist,L., Reinhardt,R., Backofen,R. and Vogel,J. (2016) Global RNA recognition patterns of post-transcriptional regulators Hfq and CsrA revealed by UV crosslinking in vivo. *EMBO J.*, **35**, 991–1011.
45. Frohlich,K.S., Papenfort,K., Berger,A.A. and Vogel,J. (2012) A conserved RpoS-dependent small RNA controls the synthesis of major porin OmpD. *Nucleic Acids Res.*, **40**, 3623–3640.
46. Pfeiffer,V., Sittka,A., Tomer,R., Tedin,K., Brinkmann,V. and Vogel,J. (2007) A small non-coding RNA of the invasion gene island (SPI-1) represses outer membrane protein synthesis from the Salmonella core genome. *Mol. Microbiol.*, **66**, 1174–1191.
47. Bilusic,I., Popitsch,N., Rescheneder,P., Schroeder,R. and Lybecker,M. (2014) Revisiting the coding potential of the E. coli genome through Hfq co-immunoprecipitation. *RNA Biol.*, **11**, 641–654.
48. Storz,G., Vogel,J. and Wassarman,K.M. (2011) Regulation by small RNAs in bacteria: expanding frontiers. *Mol. Cell*, **43**, 880–891.
49. Peschek,N., Hoyos,M., Herzog,R., Forstner,K.U. and Papenfort,K. (2019) A conserved RNA seed-pairing domain directs small RNA-mediated stress resistance in enterobacteria. *EMBO J.*, **38**, e101650.
50. Dimastrogiovanni,D., Frohlich,K.S., Bandyra,K.J., Bruce,H.A., Hohensee,S., Vogel,J. and Luisi,B.F. (2014) Recognition of the small regulatory RNA RydC by the bacterial Hfq protein. *eLife*, **3**, e05375.
51. Malecka,E.M., Strozecka,J., Sobanska,D. and Olejniczak,M. (2015) Structure of bacterial regulatory RNAs determines their performance in competition for the chaperone protein Hfq. *Biochemistry*, **54**, 1157–1170.
52. Bandyra,K.J., Sinha,D., Syrjanen,J., Luisi,B.F. and De Lay,N.R. (2016) The ribonuclease polynucleotide phosphorylase can interact with small regulatory RNAs in both protective and degradative modes. *RNA*, **22**, 360–372.
53. Rabin,R.S. and Stewart,V. (1993) Dual response regulators (NarL and NarP) interact with dual sensors (NarX and NarQ) to control nitrate- and nitrite-regulated gene expression in Escherichia coli K-12. *J. Bacteriol.*, **175**, 3259–3268.
54. Darwin,A.J., Tyson,K.L., Busby,S.J. and Stewart,V. (1997) Differential regulation by the homologous response regulators NarL and NarP of Escherichia coli K-12 depends on DNA binding site arrangement. *Mol. Microbiol.*, **25**, 583–595.
55. Myers,K.S., Yan,H., Ong,I.M., Chung,D., Liang,K., Tran,F., Keles,S., Landick,R. and Kiley,P.J. (2013) Genome-scale analysis of escherichia coli FNR reveals complex features of transcription factor binding. *PLos Genet.*, **9**, e1003565.
56. Darwin,A.J. and Stewart,V. (1996) *The NAR Modulon Systems: Nitrate and Nitrite Regulation of Anaerobic Gene Expression. In: Regulation of Gene Expression in Escherichia coli*. Springer, Boston.
57. Apirion,D. and Lassar,A.B. (1978) A conditional lethal mutant of Escherichia coli which affects the processing of ribosomal RNA. *J. Biol. Chem.*, **253**, 1738–1742.
58. Figueroa-Bossi,N., Valentini,M., Malleret,L., Fiorini,F. and Bossi,L. (2009) Caught at its own game: regulatory small RNA inactivated by an inducible transcript mimicking its target. *Genes Dev.*, **23**, 2004–2015.
59. Corcoran,C.P., Podkaminski,D., Papenfort,K., Urban,J.H., Hinton,J.C. and Vogel,J. (2012) Superfolder GFP reporters validate diverse new mRNA targets of the classic porin regulator, MicF RNA. *Mol. Microbiol.*, **84**, 428–445.
60. Wright,P.R., Richter,A.S., Papenfort,K., Mann,M., Vogel,J., Hess,W.R., Backofen,R. and Georg,J. (2013) Comparative genomics boosts target prediction for bacterial small RNAs. *Proc. Natl. Acad. Sci. U.S.A.*, **110**, E3487–E3496.
61. Wright,P.R., Georg,J., Mann,M., Sorescu,D.A., Richter,A.S., Lott,S., Kleinkauf,R., Hess,W.R. and Backofen,R. (2014) CopraRNA and IntaRNA: predicting small RNA targets, networks and interaction domains. *Nucleic Acids Res.*, **42**, W119–W123.
62. Bouvier,M., Sharma,C.M., Mika,F., Nierhaus,K.H. and Vogel,J. (2008) Small RNA binding to 5′ mRNA coding region inhibits translational initiation. *Mol. Cell*, **32**, 827–837.
63. DeMoss,J.A. and Hsu,P.Y. (1991) NarK enhances nitrate uptake and nitrite excretion in Escherichia coli. *J. Bacteriol.*, **173**, 3303–3310.
64. Fukuda,M., Takeda,H., Kato,H.E., Doki,S., Ito,K., Maturana,A.D., Ishitani,R. and Nureki,O. (2015) Structural basis for dynamic mechanism of nitrate/nitrite antiport by NarK. *Nat. Commun.*, **6**, 7097.
65. Harborne,N.R., Griffiths,L., Busby,S.J. and Cole,J.A. (1992) Transcriptional control, translation and function of the products of the five open reading frames of the Escherichia coli nir operon. *Mol. Microbiol.*, **6**, 2805–2813.
66. Bonnefoy,V. and DeMoss,J.A. (1992) Identification of functional cis-acting sequences involved in regulation of narK gene expression in Escherichia coli. *Mol. Microbiol.*, **6**, 3595–3602.
67. Warren,M.J., Bolt,E.L., Roessner,C.A., Scott,A.I., Spencer,J.B. and Woodcock,S.C. (1994) Gene dissection demonstrates that the

Escherichia coli cysG gene encodes a multifunctional protein. *Biochem. J.*, **302**, 837–844.
68. Spencer,J.B., Stolowich,N.J., Roessner,C.A. and Scott,A.I. (1993) The Escherichia coli cysG gene encodes the multifunctional protein, siroheme synthase. *FEBS Lett.*, **335**, 57–60.
69. Peakman,T., Busby,S. and Cole,J. (1990) Transcriptional control of the cysG gene of Escherichia coli K-12 during aerobic and anaerobic growth. *Eur. J. Biochem.*, **191**, 325–331.
70. Belyaeva,T., Griffiths,L., Minchin,S., Cole,J. and Busby,S. (1993) The Escherichia coli cysG promoter belongs to the 'extended -10' class of bacterial promoters. *Biochem. J.*, **296**, 851–857.
71. Lundberg,J.O., Weitzberg,E., Cole,J.A. and Benjamin,N. (2004) Nitrate, bacteria and human health. *Nat. Rev. Microbiol.*, **2**, 593–602.
72. Rivera-Chavez,F. and Baumler,A.J. (2015) The pyromaniac inside you: salmonella metabolism in the host gut. *Annu. Rev. Microbiol.*, **69**, 31–48.
73. Vazquez-Torres,A. and Baumler,A.J. (2016) Nitrate, nitrite and nitric oxide reductases: from the last universal common ancestor to modern bacterial pathogens. *Curr. Opin. Microbiol.*, **29**, 1–8.
74. Stewart,V. (1982) Requirement of Fnr and NarL functions for nitrate reductase expression in Escherichia coli K-12. *J. Bacteriol.*, **151**, 1320–1325.
75. Jayaraman,P.S., Gaston,K.L., Cole,J.A. and Busby,S.J. (1988) The nirB promoter of Escherichia coli: location of nucleotide sequences essential for regulation by oxygen, the FNR protein and nitrite. *Mol. Microbiol.*, **2**, 527–530.
76. Klahn,S., Schaal,C., Georg,J., Baumgartner,D., Knippen,G., Hagemann,M., Muro-Pastor,A.M. and Hess,W.R. (2015) The sRNA NsiR4 is involved in nitrogen assimilation control in cyanobacteria by targeting glutamine synthetase inactivating factor IF7. *Proc. Natl. Acad. Sci. U.S.A.*, **112**, E6243–E6252.
77. Zhan,Y., Yan,Y., Deng,Z., Chen,M., Lu,W., Lu,C., Shang,L., Yang,Z., Zhang,W., Wang,W. *et al.* (2016) The novel regulatory ncRNA, NfiS, optimizes nitrogen fixation via base pairing with the nitrogenase gene nifK mRNA in Pseudomonas stutzeri A1501. *Proc. Natl. Acad. Sci. U.S.A.*, **113**, E4348–E4356.
78. Hao,Y., Updegrove,T.B., Livingston,N.N. and Storz,G. (2016) Protection against deleterious nitrogen compounds: role of sigmaS-dependent small RNAs encoded adjacent to sdiA. *Nucleic. Acids. Res.*, **44**, 6935–6948.
79. Durand,S. and Storz,G. (2010) Reprogramming of anaerobic metabolism by the FnrS small RNA. *Mol. Microbiol.*, **75**, 1215–1231.
80. Waters,S.A., McAteer,S.P., Kudla,G., Pang,I., Deshpande,N.P., Amos,T.G., Leong,K.W., Wilkins,M.R., Strugnell,R., Gally,D.L. *et al.* (2017) Small RNA interactome of pathogenic E. coli revealed through crosslinking of RNase E. *EMBO J.*, **36**, 374–387.
81. Adhya,S. (2003) Suboperonic regulatory signals. *Sci. STKE*, **2003**, pe22.
82. Quax,T.E., Claassens,N.J., Soll,D. and van der Oost,J. (2015) Codon bias as a means to fine-tune gene expression. *Mol. Cell*, **59**, 149–161.
83. Warren,M.J., Roessner,C.A., Santander,P.J. and Scott,A.I. (1990) The Escherichia coli cysG gene encodes S-adenosylmethionine-dependent uroporphyrinogen III methylase. *Biochem. J.*, **265**, 725–729.
84. Balasubramanian,D. and Vanderpool,C.K. (2013) New developments in post-transcriptional regulation of operons by small RNAs. *RNA Biol*, **10**, 337–341.
85. Desnoyers,G., Morissette,A., Prevost,K. and Masse,E. (2009) Small RNA-induced differential degradation of the polycistronic mRNA iscRSUA. *EMBO J.*, **28**, 1551–1561.
86. Lalanne,J.B., Taggart,J.C., Guo,M.S., Herzel,L., Schieler,A. and Li,G.W. (2018) Evolutionary convergence of pathway-specific enzyme expression stoichiometry. *Cell*, **173**, 749–761.
87. Beisel,C.L., Updegrove,T.B., Janson,B.J. and Storz,G. (2012) Multiple factors dictate target selection by Hfq-binding small RNAs. *EMBO J.*, **31**, 1961–1974.
88. Kalamorz,F., Reichenbach,B., Marz,W., Rak,B. and Gorke,B. (2007) Feedback control of glucosamine-6-phosphate synthase GlmS expression depends on the small RNA GlmZ and involves the novel protein YhbJ in Escherichia coli. *Mol. Microbiol.*, **65**, 1518–1533.
89. Reichenbach,B., Maes,A., Kalamorz,F., Hajnsdorf,E. and Gorke,B. (2008) The small RNA GlmY acts upstream of the sRNA GlmZ in the activation of glmS expression and is subject to regulation by polyadenylation in Escherichia coli. *Nucleic Acids Res.*, **36**, 2570–2580.
90. Urban,J.H. and Vogel,J. (2008) Two seemingly homologous noncoding RNAs act hierarchically to activate glmS mRNA translation. *PLoS Biol.*, **6**, e64.
91. Deana,A. and Belasco,J.G. (2005) Lost in translation: the influence of ribosomes on bacterial mRNA decay. *Genes Dev.*, **19**, 2526–2533.
92. Hui,M.P., Foley,P.L. and Belasco,J.G. (2014) Messenger RNA degradation in bacterial cells. *Annu. Rev. Genet.*, **48**, 537–559.
93. Durand,S., Tomasini,A., Braun,F., Condon,C. and Romby,P. (2015) sRNA and mRNA turnover in Gram-positive bacteria. *FEMS Microbiol. Rev.*, **39**, 316–330.
94. Lalaouna,D., Baude,J., Wu,Z., Tomasini,A., Chicher,J., Marzi,S., Vandenesch,F., Romby,P., Caldelari,I. and Moreau,K. (2019) RsaC sRNA modulates the oxidative stress response of Staphylococcus aureus during manganese starvation. *Nucleic Acids Res.*, **47**, 9871–9887.